

# Reduced Navier-Stokes Equations Near a Flow Boundary

M. S. Kilibic<sup>1</sup>, G. B. Jacobs<sup>2,3</sup>, J. S. Hesthaven<sup>2</sup>, and G. Haller<sup>3\*</sup>

<sup>1</sup>Department of Mathematics, MIT, 77 Massachusetts Ave., Cambridge, MA 02139, USA

<sup>2</sup>Division of Applied Mathematics, Brown University, Providence, RI, 02912, USA

<sup>3</sup>Department of Mechanical Engineering, MIT, 77 Massachusetts Ave., Cambridge, MA 02139, USA

August 4, 2005

## Abstract

We derive a hierarchy of PDEs for the leading-order evolution of wall-based quantities, such as the skin-friction and the wall-pressure gradient, in two-dimensional fluid flows. The resulting *Reduced Navier-Stokes (RNS)* equations are defined on the boundary of the flow, and hence have reduced spatial dimensionality compared to the Navier-Stokes equations. This spatial reduction speeds up numerical computations and makes the equations attractive candidates for flow-control design. We prove that members of the RNS hierarchy are well-posed if appended with boundary-conditions obtained from wall-based sensors. We also derive the lowest-order RNS equations for three-dimensional flows. For several benchmark problems, our numerical simulations show close finite-time agreement between the solutions of RNS and those of the full Navier-Stokes equations.

## 1 Introduction

### 1.1 Background and motivation

The approximation of Navier-Stokes flows near a no-slip boundary was apparently first discussed in detail by Perry and Chong [11], who developed a procedure for finding the Taylor coefficients of a velocity field expanded at a boundary point. By this procedure, one can construct velocity models that are polynomials in terms of the distance from the point of expansion. The models are dynamically consistent up to any desired order, but depend on properties imposed a priori on the velocity derivatives at the wall.

Danielson and Ottino [3] used the above procedure to construct a system of ODEs for the Taylor coefficients of a velocity field at a no-slip boundary point. The ODE system becomes finite-dimensional upon truncation of the Taylor expansion; Danielson and Ottino showed that even low-order truncations may lead to ODEs with a strange attractor, a hallmark of Eulerian turbulence.

Recently, Bewley and Protas [12] proposed a less restrictive Taylor-expansion of the velocity in terms of the normal distance from the boundary. For two-dimensional flows, this procedure yields a single-variable Taylor-expansion with coefficients depending on the location along the boundary. Bewley and Protas showed that under appropriate conditions, the expansion converges in a vicinity of the wall. In addition, for incompressible flows, all Taylor coefficients can be expressed in terms of time- and wall-tangential derivatives of the wall shear (skin friction) and the wall pressure.

With the availability of accurate skin-friction and pressure sensor-arrays, the results in [12] enable local velocity reconstruction from wall-based measurements. This offers a promising tool for practical flow control, where the impact of the controller must be evaluated from wall sensors.

---

\*Corresponding author. Email: ghaller@mit.edu

## Report Documentation Page

*Form Approved*  
*OMB No. 0704-0188*

Public reporting burden for the collection of information is estimated to average 1 hour per response, including the time for reviewing instructions, searching existing data sources, gathering and maintaining the data needed, and completing and reviewing the collection of information. Send comments regarding this burden estimate or any other aspect of this collection of information, including suggestions for reducing this burden, to Washington Headquarters Services, Directorate for Information Operations and Reports, 1215 Jefferson Davis Highway, Suite 1204, Arlington VA 22202-4302. Respondents should be aware that notwithstanding any other provision of law, no person shall be subject to a penalty for failing to comply with a collection of information if it does not display a currently valid OMB control number.

1. REPORT DATE <b>04 AUG 2005</b>		2. REPORT TYPE		3. DATES COVERED <b>00-08-2005 to 00-08-2005</b>	
4. TITLE AND SUBTITLE <b>Reduced Navier-Stokes Equations Near a Flow Boundary</b>				5a. CONTRACT NUMBER	
				5b. GRANT NUMBER	
				5c. PROGRAM ELEMENT NUMBER	
6. AUTHOR(S)				5d. PROJECT NUMBER	
				5e. TASK NUMBER	
				5f. WORK UNIT NUMBER	
7. PERFORMING ORGANIZATION NAME(S) AND ADDRESS(ES) <b>Brown University, Division of Applied Mathematics, 182 George Street, Providence, RI, 02912</b>				8. PERFORMING ORGANIZATION REPORT NUMBER	
9. SPONSORING/MONITORING AGENCY NAME(S) AND ADDRESS(ES)				10. SPONSOR/MONITOR'S ACRONYM(S)	
				11. SPONSOR/MONITOR'S REPORT NUMBER(S)	
12. DISTRIBUTION/AVAILABILITY STATEMENT <b>Approved for public release; distribution unlimited</b>					
13. SUPPLEMENTARY NOTES					
14. ABSTRACT					
15. SUBJECT TERMS					
16. SECURITY CLASSIFICATION OF:			17. LIMITATION OF ABSTRACT	18. NUMBER OF PAGES <b>30</b>	19a. NAME OF RESPONSIBLE PERSON
a. REPORT <b>unclassified</b>	b. ABSTRACT <b>unclassified</b>	c. THIS PAGE <b>unclassified</b>			

Feedback control, however, requires more than just an observation of the output: a model for the evolution of the flow is also crucial. The Bewley–Protas results offer hope that, at least near the wall, such models are reducible to depend only on the skin friction and wall pressure.

Further underlying the need for such reduced flow models, typical performance objectives in flow-control are often phrased directly in terms of skin friction and wall pressure, not velocity. Examples include pressure–recovery enhancement in diffusers and surface–drag reduction on submarines. The former aims to maximize the integral of the wall-pressure gradient; the latter to minimize the integral of the skin friction. In both cases, a qualitative prediction for the evolution of the underlying quantity is more beneficial than a highly accurate but complex numerical model.

## 1.2 Main results

Motivated by the above, here we study how the dynamics of wall-based quantities, such as the wall-shear  $\tau(x)$  and the wall-pressure gradient  $\gamma(x)$ , can be modelled and predicted in two-dimensional Navier-Stokes flows. Our main result is a hierarchy of models, the *Reduced Navier-Stokes (RNS) equations*, that describe the evolution of the above quantities at different levels of accuracy. Since the RNS equations are defined on the flow boundary, they only have one spatial dimension, the wall coordinate  $x$ . This dimensional reduction results in computation times that are significantly shorter than those of direct Navier–Stokes simulations.

Solving the RNS equations requires updated boundary conditions for  $\tau$  and  $\gamma$  at two  $x$ -locations,  $x_1$  and  $x_2$ . Thus,  $x_1$  and  $x_2$  must either be points with a priori known velocity derivatives (e.g., corner points), or must lie within distributed skin-friction and wall-pressure sensor arrays. In either case, the RNS equations provide qualitative prediction for the evolution of  $\tau(x)$  and  $\gamma(x)$  over the whole interval  $(x_1, x_2)$ . The prediction necessarily deteriorates over time; solving the RNS equations over longer times, therefore, requires periodic re-initialization by sampling  $\tau(x)$  and  $\gamma(x)$  from sensors distributed over  $(x_1, x_2)$ .

We derive three members of the RNS hierarchy explicitly; these evolution equations are obtained from cubic, quartic, and quintic truncations of the Taylor expansion of the wall-tangential velocity component. We prove that these three RNS equations and all higher-order RNS systems are well-posed, i.e., admit unique solutions that depend continuously on the initial data. We also derive the lowest-order RNS equation for three-dimensional flows, and discuss the relevance of the two-dimensional RNS equations in select flow-control problems.

We present evidence for the accuracy of the RNS equations by comparing their numerical solution to classic solutions of the Navier-Stokes equations. These classic solutions include a viscous channel flow, the Blasius boundary layer solution, viscous flow near a stagnation point, and an oscillating flow over an infinite plate. We finally compare the direct numerical simulation of a lid-driven cavity flow to that of the RNS equations. In all cases, we observe close quantitative agreement on short to intermediate time scales, and qualitative accuracy over longer time scales.

## 2 RNS equations for two-dimensional flows

Consider the two-dimensional Navier-Stokes equations

$$\begin{aligned}\partial_t u + u_x u + u_y v &= -\frac{1}{\rho} p_x + \nu(u_{xx} + u_{yy}), \\ \partial_t v + v_x u + v_y v &= -\frac{1}{\rho} p_y + \nu(v_{xx} + v_{yy}),\end{aligned}\tag{1}$$

where  $(u(x, y, t), v(x, y, t))$  is a velocity field satisfying the incompressibility condition

$$u_x + v_y = 0,\tag{2}$$

and the no-slip boundary condition

$$u(x, 0, t) = v(x, 0, t) = 0 \quad (3)$$

at the  $y = 0$  boundary. In (1),  $p(x, y, t)$  denotes the pressure, and  $\nu$  and  $\rho$  are the kinematic viscosity and the density of the fluid.

We seek to understand the evolution of the *skin-friction field*

$$\tau(x, t) = \rho\nu u_y(x, 0, t),$$

and the *wall-pressure-gradient field*

$$\gamma(x, t) = p_x(x, 0, t) = \rho\nu u_{yy}(x, 0, t). \quad (4)$$

As auxiliary variables to be used later, we also introduce

$$\sigma(x, t) = \rho\nu u_{yyy}(x, 0, t), \quad \lambda(x, t) = \rho\nu u_{yyyy}(x, 0, t), \quad \eta(x, t) = \rho\nu u_{yyyyy}(x, 0, t).$$

With the above variables, the Taylor expansion of  $u(x, y, t)$  near the  $y = 0$  boundary can be written as

$$u(x, y, t) = \frac{1}{\nu\rho} \left[ \tau(x, t)y + \frac{1}{2}\gamma(x, t)y^2 + \frac{1}{6}\sigma(x, t)y^3 + \frac{1}{24}\lambda(x, t)y^4 + \frac{1}{120}\eta(x, t)y^5 + \mathcal{O}(y^6) \right]. \quad (5)$$

Subtracting the  $x$ -derivative of the second equation in (1) from the  $y$ -derivative of the first equation, we obtain the vorticity-transport equation

$$\partial_t(u_y - v_x) + u(u_{xy} - v_{xx}) + v(u_{xx} + u_{yy}) = \nu(2u_{xxy} + u_{yyy} - v_{xx}), \quad (6)$$

from which we shall derive approximate expressions for the evolution of the Taylor coefficients in (5).

## 2.1 The cubic RNS equations

Setting  $y = 0$  in equation (6) yields

$$\tau_t = \nu(2\tau_{xx} + \sigma). \quad (7)$$

Differentiating (6) with respect to  $y$  and using the incompressibility condition (2) leads to

$$\begin{aligned} & \partial_t(u_{xx} + u_{yy}) + u_y(u_{xy} - v_{xx}) + u(u_{xyy} + u_{xxx}) - u_x(u_{xx} + u_{yy}) + v(u_{xxy} + u_{yyy}) \\ &= \nu(2u_{xxyy} + u_{yyyy} + u_{xxxx}). \end{aligned} \quad (8)$$

After setting  $y = 0$  in (8), we obtain

$$\gamma_t + \frac{1}{\nu\rho}\tau\tau_x = \nu(2\gamma_{xx} + \nu\rho u_{yyyy}). \quad (9)$$

Finally, differentiating (8) with respect to  $y$ , we find that

$$\begin{aligned} & \partial_t(u_{xxy} + u_{yyy}) + u_{yy}(u_{xy} - v_{xx}) + u_y(u_{xyy} + u_{xxx}) + u_y(u_{xyy} + u_{xxx}) \\ & + u(u_{xyyy} + u_{xxx}) - u_{xy}(u_{xx} + u_{yy}) - 2u_x(u_{yyy} + u_{xxy}) + v(u_{yyyy} + u_{xxyy}) \\ &= \nu(2u_{xxyyy} + u_{yyyyy} + u_{xxxxy}). \end{aligned} \quad (10)$$

Setting  $y = 0$  in this last equation, we obtain

$$[\partial_t(u_{xxy} + u_{yyy}) + 2u_y u_{yyx}]_{y=0} = \nu(2u_{xxyyy} + u_{yyyyy} + u_{xxxxy})_{y=0}. \quad (11)$$

At the same time, the second  $x$ -derivative of (6) taken at  $y = 0$  is

$$(\partial_t u_{xxy})_{y=0} = \nu (2u_{xxxxxy} + u_{xxyyy})_{y=0}. \quad (12)$$

Combining (11) and (12) gives

$$\sigma_t + \frac{2}{\nu\rho} \tau \gamma_x = \nu (\sigma_{xx} + \nu\rho u_{yyyyy} - \tau_{xxxx}). \quad (13)$$

We now assume that the velocity component  $u(x, y, t)$  is well approximated by its third-order Taylor expansion near the  $y = 0$  boundary; in other words, we truncate the expansion (5) at cubic order. Under this approximation, equations (7), (9), and (13) yield the *cubic RNS equations*

$$\begin{aligned} \tau_t &= 2\nu\tau_{xx} + \nu\sigma, \\ \gamma_t &= 2\nu\gamma_{xx} - \frac{1}{\nu\rho} \tau\tau_x, \\ \sigma_t &= \nu\sigma_{xx} - \nu\tau_{xxxx} - \frac{2}{\nu\rho} \tau\gamma_x. \end{aligned} \quad (14)$$

To this nonlinear system of PDEs, we add the boundary and initial conditions

$$\begin{aligned} \tau(0, t) &= T_0(t), \quad \tau(L, t) = T_1(t), \quad \tau(x, t_0) = \tau^0(x), \\ \gamma(0, t) &= G_0(t), \quad \gamma(L, t) = G_1(t), \quad \gamma(x, t_0) = \gamma^0(x), \\ \sigma(0, t) &= S_0(t), \quad \sigma(L, t) = S_1(t), \quad \sigma(x, t_0) = \sigma^0(x). \end{aligned} \quad (15)$$

The initial and boundary conditions for  $\tau$  may be obtained from distributed skin-friction sensors; the same conditions for  $\gamma$  can be measured by distributed pressure sensors. Realistic sensors do not exist for measuring  $\sigma$  directly, but distributed skin-friction sensors can be used to find the values of  $\sigma$  from the relations

$$\sigma(0, t) = \dot{T}_0(t) - 2\nu\tau_{xx}(0, t), \quad \sigma(L, t) = \dot{T}_L(t) - 2\nu\tau_{xx}(L, t), \quad \sigma(x, t_0) = \dot{\tau}(x, t_0) - 2\nu\tau_{xx}^0(x).$$

The solvability of the cubic RNS equations (14) is guaranteed by the following result.

**Theorem 2.1.** *The cubic RNS equations (14) with the boundary and initial conditions (15) are well-posed: they admit unique solutions with continuous dependence on initial data on the function space  $H^3[0, L] \times H^2[0, L] \times H^1[0, L]$ .*

*Proof:* See Appendix 7.1.

The advantage of the cubic RNS equations (14) is that they are defined on the one-dimensional spatial domain  $[0, L]$ , as opposed to the Navier-Stokes equations (1) that are defined on a two-dimensional domain. System (14), however, cannot be solved independently: its time-dependent boundary conditions are to be obtained from pressure- and skin-friction sensors at the boundary. In addition, a distributed skin-friction and pressure measurement at  $t = 0$  is necessary to identify the initial condition.

Since the system (14) is obtained from a Taylor-series truncation of the original velocity field, it will only approximate true Navier-Stokes solutions for finite times. As a result, (14) must be periodically re-initialized for its solutions to stay accurate. Our main motivation is controller design, for which the simplicity and the short-term predictive power of (14) is more important than its long-term accuracy.

## 2.2 The quartic RNS equations

For increased accuracy, we now derive a higher-order approximation for the evolution of velocity derivatives at the wall. Differentiating (10) with respect to  $y$ , we obtain

$$\begin{aligned} & \partial_t (u_{xxyy} + u_{yyyy}) - u_{yyy}v_{xx} + u_{yy} (2u_{xyy} + 2u_{xxx}) + 3u_y (u_{xyyy} + u_{xxyy}) \\ & + u (u_{xyyyy} + u_{xxxyy}) - u_{xyy}u_{xx} - 3u_{xy}u_{xxy} \\ & - 2u_{xy}u_{yyy} - 3u_x (u_{yyyy} + u_{xxyy}) + v (u_{yyyyy} + u_{xxyyy}) \\ = & \nu (2u_{xxyyyy} + u_{yyyyyy} + u_{xxxxyy}). \end{aligned} \quad (16)$$

Setting  $y = 0$  in this equation gives

$$\begin{aligned} & [\partial_t (u_{xxyy} + u_{yyyy}) + 2u_{yy}u_{xyy} + 3u_y (u_{xyyy} + u_{xxyy}) - 3u_{xy}u_{xxy} - 2u_{xy}u_{yyy}]_{y=0} \\ = & \nu (2u_{xxyyyy} + u_{yyyyyy} + u_{xxxxyy})_{y=0}. \end{aligned} \quad (17)$$

Next, we differentiate (8) twice with respect to  $x$  and set  $y = 0$  to obtain

$$\begin{aligned} & [\partial_t u_{yyxx} + 3u_{xy}u_{xxy} + u_y u_{xxx}]_{y=0} \\ = & \nu (2u_{xxxxyy} + u_{xxyyyy} + u_{xxxxxx})_{y=0}. \end{aligned} \quad (18)$$

Subtracting (18) from (17) then gives

$$\begin{aligned} & [\partial_t u_{yyyy} + 2u_{yy}u_{xyy} + u_y (3u_{xyyy} + 2u_{xxyy}) - 6u_{xy}u_{xxy} - 2u_{xy}u_{yyy}]_{y=0} \\ = & \nu (u_{xxyyyy} + u_{yyyyyy} - u_{xxxxyy})_{y=0}, \end{aligned}$$

or, equivalently,

$$\begin{aligned} & \partial_t \lambda + \frac{2}{\nu\rho} \gamma \gamma_x + \frac{1}{\nu\rho} \tau (3\sigma_x + 2\tau_{xx}) - \frac{6}{\nu\rho} \tau_x \tau_{xx} - \frac{2}{\nu\rho} \tau_x \sigma \\ = & \nu (\lambda_{xx} + \nu\rho u_{yyyyyy} - \gamma_{xxx}). \end{aligned}$$

We now assume that the velocity component  $u(x, y, t)$  is well approximated by its forth-order Taylor expansion near the boundary, i.e., we truncate the expansion (5) at quartic order. Under this approximation, equations (7), (9), and (13) can be summarized in the *quartic RNS equations*

$$\begin{aligned} \tau_t &= 2\nu\tau_{xx} + \nu\sigma, \\ \gamma_t &= 2\nu\gamma_{xx} + \nu\lambda - \frac{1}{\nu\rho} \tau \tau_x, \\ \sigma_t &= \nu\sigma_{xx} - \nu\tau_{xxx} - \frac{2}{\nu\rho} \tau \gamma_x, \\ \lambda_t &= \nu\lambda_{xx} - \nu\gamma_{xxx} - \frac{2}{\nu\rho} \gamma \gamma_x - \frac{1}{\nu\rho} \tau (3\sigma_x + 2\tau_{xx}) + \frac{6}{\nu\rho} \tau_x \tau_{xx} + \frac{2}{\nu\rho} \tau_x \sigma, \end{aligned} \quad (19)$$

with the initial and boundary conditions

$$\begin{aligned} \tau(0, t) &= T_0(t), \quad \tau(L, t) = T_1(t), \quad \tau(x, t_0) = \tau^0(x), \\ \gamma(0, t) &= G_0(t), \quad \gamma(L, t) = G_1(t), \quad \gamma(x, t_0) = \gamma^0(x), \\ \sigma(0, t) &= S_0(t), \quad \sigma(L, t) = S_1(t), \quad \sigma(x, t_0) = \sigma^0(x), \\ \lambda(0, t) &= L_0(t), \quad \lambda(L, t) = L_1(t), \quad \lambda(x, t_0) = \lambda^0(x). \end{aligned} \quad (20)$$

The boundary and initial conditions for  $\lambda$  can again be obtained from distributed skin-friction and pressure measurements:

$$\begin{aligned} \lambda(0, t) &= \left[ \dot{G}_0(t) - 2\nu\gamma_{xx}(0, t) + T_0(t)\tau_x(0, t) / (\nu\rho) \right] / \nu, \\ \lambda(L, t) &= \left[ \dot{G}_1(t) - 2\nu\gamma_{xx}(L, t) + T_1(t)\tau_x(L, t) / (\nu\rho) \right] / \nu, \\ \lambda(x, t_0) &= \dot{\gamma}(x, t_0) - 2\nu\gamma_{xx}^0(x) + \tau^0(x)\tau_x^0(x) / (\nu\rho). \end{aligned}$$

The solvability of the quartic RNS equations (14) is guaranteed by the following result.

**Theorem 2.2.** *The quartic RNS equations (19) with the boundary and initial conditions (20) are well-posed on the function space  $H^4[0, L] \times H^3[0, L] \times H^2[0, L] \times H^1[0, L]$ .*

*Proof:* See Appendix 7.2

Note that the evolution of the pressure gradient and the skin friction remain independent in Stokes flows even after the addition of higher order terms. The same conclusion will hold for any higher-order RNS equation. In those higher-order equations, the only further change is the appearance of linear coupling terms to higher-order  $y$ -derivatives of  $u$ . This suggests that the first robust enough model for both the skin friction and the pressure gradient is the quartic model.

### 2.3 Higher-order RNS equations

In order to derive an  $n$ th order approximation for the evolution of flow-derivatives at the wall, we subtract the second  $x$ -derivative of the order  $n-2$  RNS equations from the  $(n-3)$ -order  $y$ -derivative of equation (10). Setting  $y = 0$  in the resulting equation and neglecting  $y$ -derivatives of  $u$  higher in order than  $n$ , we obtain the  $n$ th-order RNS equations. For example, the *quintic RNS equations* take the form

$$\begin{aligned}
\tau_t &= 2\nu\tau_{xx} + \nu\sigma, \\
\gamma_t &= 2\nu\gamma_{xx} + \nu\lambda - \frac{1}{\nu\rho}\tau\tau_x, \\
\sigma_t &= \nu\sigma_{xx} - \nu\tau_{xxxx} + \nu\eta - \frac{2}{\nu\rho}\tau\gamma_x, \\
\lambda_t &= \nu\lambda_{xx} - \nu\gamma_{xxx} - \frac{2}{\nu\rho}\gamma\gamma_x - \frac{1}{\nu\rho}\tau(3\sigma_x + 2\tau_{xxx}) + \frac{6}{\nu\rho}\tau_x\tau_{xx} + \frac{2}{\nu\rho}\tau_x\sigma, \\
\eta_t &= \nu\eta_{xx} + \nu\tau_{xxxxx} + \frac{1}{\nu\rho}[(5\lambda + 8\gamma_{xx})\tau_x - 5\gamma(\sigma_x + \tau_{xxx}) - \tau(4\lambda_x + 3\gamma_{xxx}) + 5\tau_{xx}\gamma_x],
\end{aligned} \tag{21}$$

with appropriate boundary and initial conditions.

Our regularity results extend to the solutions of higher-order RNS equations:

**Theorem 2.3.** *For any  $n \geq 3$ , the  $n$ th-order RNS equations are well-posed on the function space  $H^n[0, L] \times \dots \times H^1[0, L]$ .*

*Proof:* See Appendix 7.2.

## 3 RNS equations for three-dimensional flows

Although the focus of the present paper is two-dimensional flows, we briefly discuss here how analogous equations can be derived in three-dimensions. We start with the three-dimensional Navier-Stokes equations

$$\begin{aligned}
u_t + u_x u + u_y v + u_z w &= -\frac{1}{\rho}p_x + \nu(u_{xx} + u_{yy} + u_{zz}) \\
v_t + v_x u + v_y v + v_z w &= -\frac{1}{\rho}p_y + \nu(v_{xx} + v_{yy} + v_{zz}) \\
w_t + w_x u + w_y v + w_z w &= -\frac{1}{\rho}p_z + \nu(w_{xx} + w_{yy} + w_{zz})
\end{aligned} \tag{22}$$

where  $(u(x, y, z, t), v(x, y, z, t), w(x, y, z, t))$  is a velocity field satisfying the incompressibility condition

$$u_x + v_y + w_z = 0,$$

and the no-slip boundary condition

$$u(x, y, 0, t) = 0, \quad v(x, y, 0, t) = 0.$$

In (22),  $p(x, y, z, t)$  denotes the pressure, and  $\nu$  and  $\rho$  are the kinematic viscosity and the density of the fluid.

The *skin-friction field* is now defined as

$$(\tau^1(x, y, t), \tau^2(x, y, t)) = (\rho\nu u_z, \rho\nu v_z)|_{z=0},$$

and the wall-pressure-gradient field is equal to

$$\begin{aligned} (\gamma^1(x, y, t), \gamma^2(x, y, t)) &= (p_x(x, y, 0, t), p_y(x, y, 0, t)) \\ &= (\rho\nu u_{zz}, \rho\nu v_{zz})|_{z=0}. \end{aligned}$$

As auxiliary variables to be used later, we also introduce

$$\begin{aligned} (\lambda^1, \lambda^2) &= (\rho\nu u_{zzz}, \rho\nu v_{zzz})|_{z=0}, \\ (\sigma^1, \sigma^2) &= (\rho\nu u_{zzzz}, \rho\nu v_{zzzz})|_{z=0}. \end{aligned}$$

With these variables, the Taylor expansion of  $u(x, y, z, t)$  and  $v(x, y, z, t)$  at the boundary  $z = 0$  can be written as

$$\begin{aligned} u(x, y, z, t) &= \frac{1}{\rho\nu} [\tau^1(x, y, t)z + \frac{1}{2}\gamma^1(x, y, t)z^2 + \frac{1}{6}\sigma^1(x, y, t)z^3 + \frac{1}{24}\lambda^1(x, y, t)z^4 + O(z^5)], \\ v(x, y, z, t) &= \frac{1}{\rho\nu} [\tau^2(x, y, t)z + \frac{1}{2}\gamma^2(x, y, t)z^2 + \frac{1}{6}\sigma^2(x, y, t)z^3 + \frac{1}{24}\lambda^2(x, y, t)z^4 + O(z^5)]. \end{aligned} \quad (23)$$

As we show in Appendix B, the truncation of the expansion (23) at cubic order leads to the *three-dimensional cubic RNS equation*

$$\begin{aligned} \tau_t^1 &= 2\nu\tau_{xx}^1 + \nu\tau_{yy}^1 + \nu\tau_{xy}^2 + \nu\sigma^1, \\ \tau_t^2 &= 2\nu\tau_{yy}^2 + \nu\tau_{xx}^2 + \nu\tau_{xy}^1 + \nu\sigma^2, \\ \gamma_t^1 &= \nu(2\gamma_{xx}^1 + \gamma_{yy}^1 + \lambda^1 + \gamma_{xy}^2) - \frac{1}{\nu\rho}(\tau^1\tau_x^1 - 2\tau_y^1\tau^2 - \tau^1\tau_y^2), \\ \gamma_t^2 &= \nu(2\gamma_{yy}^2 + \gamma_{xx}^2 + \lambda^2 + \gamma_{xy}^1) - \frac{1}{\nu\rho}(\tau^2\tau_y^2 - 2\tau_x^2\tau^1 - \tau^2\tau_x^1), \\ \sigma_t^1 &= -\nu[3\tau_{xxx}^1 + 3\tau_{yyx}^1 + \sigma_{xx}^1 + 3\tau_{xxy}^2 + 3\tau_{yyx}^2 + 2\sigma_{xy}^2 - \sigma_{yy}^1] \\ &\quad + \frac{1}{\nu\rho}[-2\gamma_x^1\tau^1 - 3\gamma_y^1\tau^2 - 3\tau_y^1\gamma^2 + 3\gamma^1\tau_y^2 + \tau^1\gamma_y^2 - 3\tau_{xx}^1\tau^1] \\ &\quad + \frac{1}{\nu\rho}[-3\tau_{xy}^2\tau^1 + 3\tau_{xy}^1\tau^2 + 3\tau_{yy}^2\tau^2 + 3(\tau_x^1)^2 + 6\tau_x^1\tau_y^2 + 3(\tau_y^2)^2], \\ \sigma_t^2 &= -\nu[3\tau_{yyy}^2 + 3\tau_{yyx}^2 + \sigma_{yy}^2 + 3\tau_{xyy}^1 + 3\tau_{yxx}^1 + 2\sigma_{xy}^1 - \sigma_{xx}^2] \\ &\quad + \frac{1}{\nu\rho}[-2\gamma_y^2\tau^2 - 3\gamma_x^2\tau^1 - 3\tau_x^2\gamma^1 + 3\gamma^2\tau_x^1 + \tau^2\gamma_x^1 - 3\tau_{yy}^2\tau^2] \\ &\quad + \frac{1}{\nu\rho}[-3\tau_{xy}^1\tau^2 + 3\tau_{xy}^2\tau^1 + 3\tau_{xx}^1\tau^1 + 3(\tau_x^1)^2 + 6\tau_x^1\tau_y^2 + 3(\tau_y^2)^2]. \end{aligned} \quad (24)$$

## 4 $\tau - \gamma$ formulation and flow control

Here we briefly discuss the relevance of the RNS equations in flow modelling and control. First, we recalling that all derivatives of an incompressible velocity field at a no-slip wall can be expressed in terms of the skin friction, pressure, their wall gradients, and their time derivatives (see Bewley and Protas [12]), This implies that (14) can be re-written as a two-dimensional set of PDEs for  $\tau$  and  $\gamma$ .

Indeed, differentiating the first equation of (14) in time gives

$$\begin{aligned}\tau_{tt} &= 2\nu\tau_{xxt} + \nu\sigma_t \\ &= 2\nu\tau_{xxt} + \nu \left[ \nu \left( \frac{1}{\nu}\tau_{xxt} - 2\tau_{xxx} \right) - \nu\tau_{xxx} - \frac{2}{\nu\rho}\tau\gamma_x \right],\end{aligned}$$

which, combined with the second equation of (14), gives the system of PDEs

$$\begin{aligned}\tau_{tt} &= 3\nu\tau_{xxt} - 3\nu^2\tau_{xxx} - \frac{2}{\rho}\tau\gamma_x, \\ \gamma_t &= 2\nu\gamma_{xx} - \frac{1}{\nu\rho}\tau\tau_x,\end{aligned}\tag{25}$$

the  $\tau - \gamma$  form of the cubic RNS equation. A similar reduction transforms the quartic RNS system (19) to the  $\tau - \gamma$  form

$$\begin{aligned}\tau_{tt} &= 3\nu\tau_{txx} - 3\nu^2\tau_{xxx} - \frac{2}{\rho}\tau\gamma_x, \\ \gamma_{tt} &= 3\nu\gamma_{txx} - 3\nu^2\gamma_{xxx} + \frac{5}{\rho}\tau_x\tau_{xx} + \frac{5}{\rho}\tau\tau_{xxx} - \frac{2}{\rho}\gamma\gamma_x - \frac{4}{\nu\rho}\tau\tau_{tx} + \frac{1}{\nu\rho}\tau_x\tau_t.\end{aligned}\tag{26}$$

The  $\tau - \gamma$  formulations (25) and (26) offer low-order approximations for the evolution of the skin friction and the wall-pressure gradient. Such approximations are useful in flow control problems where the cost function only depends on  $\tau$  or  $\gamma$ .

For instance, if  $x \in [0, L]$  varies on a wall segment connecting the inlet and the outlet of a diffuser (see Fig. 1a), then losses in the diffuser are measured by the pressure recovery

$$C_p = \frac{p(L, 0, t) - p(0, 0, t)}{\frac{1}{2}\rho u_{\text{in}}^2(t)},$$

with  $u_{\text{in}}$  denoting the mean inflow velocity. The losses will be minimal if  $C_p$  is maximal. Assuming

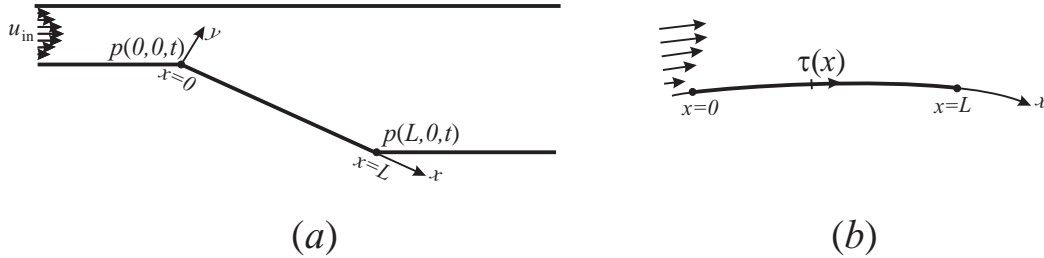


Figure 1: Possible domains of definition for the RNS equations in flow control problems. (a) Inclined wall section of a two-dimensional diffuser (b) Wall section of a two-dimensional streamlined body.

constant-in-time inflow conditions,  $C_p$  will be maximal if  $p(L, 0, t) - p(0, 0)$  is maximal. Thus, to minimize losses in the diffuser, the time-average of the cost function

$$C_\gamma(t) = \int_0^L \gamma(x, t) dx$$

is to be maximized.

Another relevant example is surface drag reduction over the boundary section  $[0, L]$  of a streamlined body (see Fig. 1b). Since the surface drag force is the integral of the wall shear along the wall, minimizing the average of the cost function

$$C_\tau(t) = \int_0^L \tau(x, t) dx,$$

minimizes surface drag over  $[0, L]$ .

## 5 Numerical study of the RNS equations

Here we show by examples that the cubic, quartic, and quintic RNS solutions approximate true Navier-Stokes solutions well over characteristic time intervals. The examples include a channel flow, a Blasius boundary layer flow, a viscous flow near a stagnation point, an oscillating flow above an infinite plane, and a lid-driven cavity flow.

In the first four examples, the Navier-Stokes equations admit exact or simplified steady-state solutions. We use these steady-state solutions as initial conditions for the RNS equations, and monitor how the solutions obtained this way deviate from the exact steady-state solutions. In our last example, we compare direct numerical solutions of the Navier-Stokes and the RNS equations. In this case, the boundary conditions for the RNS equations are a priori known: the normal derivatives of the  $u$ -velocity are zero at the corners of the lid-driven cavity.

We use a Chebyshev spectral scheme for the spatial approximation of (14), (19), and (21). We choose this method for its high accuracy and for its ability to treat Dirichlet boundary conditions (see Canuto et al. [2]). For temporal integration, we use a second-order implicit Crank-Nicholson scheme (Canuto et al. [2]) combined with a Newton-Krylov solver (Kelley [7]). We present our simulation results using the nondimensional (convective) time

$$\bar{t} = tu_0/L_0,$$

where  $u_0$  is a characteristic velocity and  $L_0$  is a characteristic length.

### Channel flow

#### *Analytical solution*

For a laminar flow between two parallel plates at distance  $L$ , the Navier-Stokes equations (1) simplify to

$$\nu u_{yy} = \frac{1}{\rho} p_x, \tag{27}$$

if we assume that the vertical velocity  $v$  vanishes, and  $u$  does not vary with  $x$ . Consequently,  $p_x \equiv p_x^0$  is a constant.

Integrating (27) with respect to  $y$  and using the symmetry condition  $u_y(x, L/2) = 0$  leads to

$$u_y(x, y) = \frac{1}{\nu\rho} p_x^0 (y - L/2). \tag{28}$$

Integrating once more and using the no-slip condition  $u = 0$  at  $y = 0$  yields

$$u(x, y) = \frac{1}{2\nu\rho} p_x^0 (y^2 - Ly). \tag{29}$$

Setting  $u(x, L/2) = u_{\max}$  then gives

$$p_x^0 = -\frac{8u_{\max}\nu\rho}{L^2}, \tag{30}$$

thus the solution of (27) can be written as

$$u(x, y) = -4u_{\max} \left[ \left( \frac{y}{L} \right)^2 - \frac{y}{L} \right]. \quad (31)$$

#### Validation

From (31), we obtain

$$\tau_{\text{exact}} = -\frac{4\rho\nu u_{\max}}{L}, \quad \gamma_{\text{exact}} = -\frac{8u_{\max}\nu\rho}{L^2}, \quad \sigma_{\text{exact}} = 0, \quad \lambda_{\text{exact}} = 0. \quad (32)$$

As a direct substitution into (14) and (19) shows, (32) is an exact solution of the cubic and quartic RNS equations. This was to be expected, because the solution (31) is exactly equal to its cubic and quartic Taylor-expansion in  $y$ .

In practice, however, initial conditions for the RNS equations are determined from sensors and hence are subject to measurement errors. We emulate such errors by selecting the perturbed initial condition

$$\tau = \tau_{\text{exact}} [1 + \epsilon \sin(2.0\pi x)], \quad \epsilon \ll 1, \quad (33)$$

in our RNS simulation instead of the exact steady-state given in (32). We select the parameters  $u_{\max} = 1 \text{ m/s}$ ,  $\nu = 0.01 \text{ m}^2/\text{s}$ , and  $\rho = 1.0 \text{ kg/m}^3$  in our simulations.

At this low Reynolds number ( $Re = u_{\max}L/\nu = 10$ ), the full Navier-Stokes equations damp out the perturbation in (33) and the flow returns to steady state. By contrast, the cubic RNS equations produce slowly growing oscillations about the steady state for the perturbed initial condition (33). Positive news on the growth is that it is weak: it does not exceed the order of the perturbation on times scales of  $\mathcal{O}(1)$ . This can be seen in Fig. 2, where the percentage error in  $\tau$  and  $\gamma$  are plotted for different RNS equations.

As seen from Fig. 2, the quartic RNS equations limit the error growth better for  $\tau$ . The quintic RNS equations (21) provide further improvement for  $\bar{t} < 1$ , but for larger times, the error grows faster. For  $\bar{t} > 5$ , the error exceeds the order of the perturbation, and hence the RNS equations have to be re-initialized. Interestingly, increasing the order of the RNS equation results in growing errors for  $\gamma$ ; the errors, however, still remain below 1% for times up to  $\bar{t} = 3$ .

Despite the growing errors, qualitative accuracy of the RNS equations persists for extended times. Specifically, qualitative correctness holds up to  $\bar{t} = 7$  in the cubic and quartic case, and up to  $\bar{t} = 5$  in the quintic case (see Fig. 3).

## Blasius boundary layer

### Similarity solution

Here we consider a similarity solution to the zero-pressure-gradient boundary layer over a flat plate accredited to Blasius (White [13]). For this flow, the Prandtl boundary-layer equations give

$$u(x, y) = Uf'(\xi), \quad |v(x, y)| \ll |u(x, y)|, \quad (34)$$

where  $U$  is a reference velocity outside the boundary layer, prime denotes differentiation with respect to the variable  $\xi = \frac{y}{x} \sqrt{\frac{Ux}{\nu}}$ , and  $f$  satisfies the ODE

$$2f''' + ff' = 0. \quad (35)$$

The boundary conditions for  $f$  are  $f(0) = f'(0) = 0$  and  $f'(\infty) \rightarrow 1$ . Solving (35) with these boundary conditions gives  $f''(0) = 0.33206$ . From (34), we obtain

$$\tau_{\text{exact}}(x) = \rho U \sqrt{\frac{\nu U}{x}} f''(0), \quad \gamma_{\text{exact}} = 0, \quad \sigma_{\text{exact}} = 0, \quad \lambda_{\text{exact}}(x) = \frac{\rho U^3}{2\nu x^2} f''^2(0), \quad \eta_{\text{exact}} = 0. \quad (36)$$

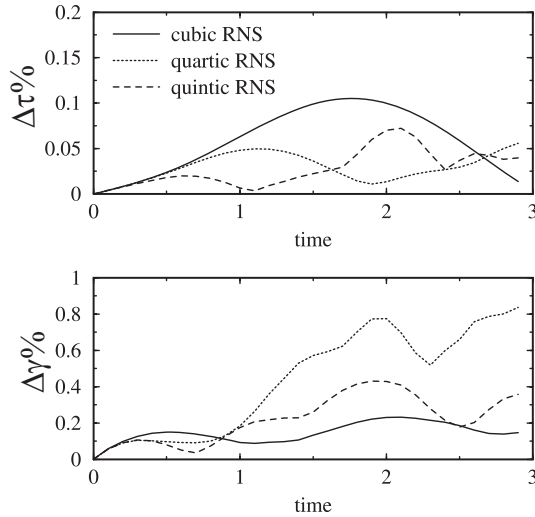


Figure 2: RNS simulations for  $\tau$  and  $\gamma$  in the perturbed channel flow with  $\epsilon = 10^{-3}$ . The percentage error for  $\tau$  is obtained as  $\Delta\tau\% = \frac{100}{N} \left[ \sum_{i=1}^N |\tau - \tau_i| \right] / \max_i |\tau_i|$  where  $\tau_1, \dots, \tau_N$  are the  $\tau$  values at  $N$  gridpoints  $x_1, \dots, x_N \in [0, 1]$ ; the definition of  $\Delta\gamma\%$  is similar.

#### Validation

We use (36) to obtain initial and boundary conditions for our simulation of the RNS equations (14), (19), and (21). We solve these equations over the spatial interval  $x \in [1, 2]$  with  $U = 1$  m/s,  $\nu = 10^{-3}$  m<sup>2</sup>/s, and  $\rho = 1.0$  kg/m<sup>3</sup>. For these parameter values, the Reynolds number is  $\text{Re} = 10^3$ , at which the boundary-layer equations are a good approximation to the Navier-Stokes equations, and hence can be compared to corresponding RNS solutions. Figure 4 shows such a comparison with the percentage error in  $\tau$  and  $\gamma$  for the cubic, quartic, and quintic RNS equations.

The error growth is faster than in the previous channel flow example, but still remains below 1% up to one convective time unit. Notably, the error in the quartic RNS is now significantly less than in the cubic RNS. The quintic RNS, however, is less accurate than the quartic, because the terms neglected in the boundary layer approximation vanish in the quartic RNS, but not in the quintic RNS.

For this example, the qualitative accuracy of the RNS systems is evidenced by Fig. 5. Even the cubic RNS solutions remain qualitatively accurate up to  $\bar{t} = 2$  convective time units, but the quartic RNS systems performs significantly better.

## Viscous flow near a stagnation point

#### Similarity solution

For a viscous stagnation point flow, the Navier-Stokes equations (1) yield the similarity solution

$$u(x, y) = BxF(\xi), \quad (37)$$

where  $F$  satisfies the ODE

$$F''' + FF'' + 1 - F'^2 = 0, \quad (38)$$

with prime denoting differentiation with respect to  $\xi = y\sqrt{\frac{B}{\nu}}$ . The parameter  $B$  is proportional to the ratio of a reference velocity  $U$  and a reference length  $L$  (White [13]).

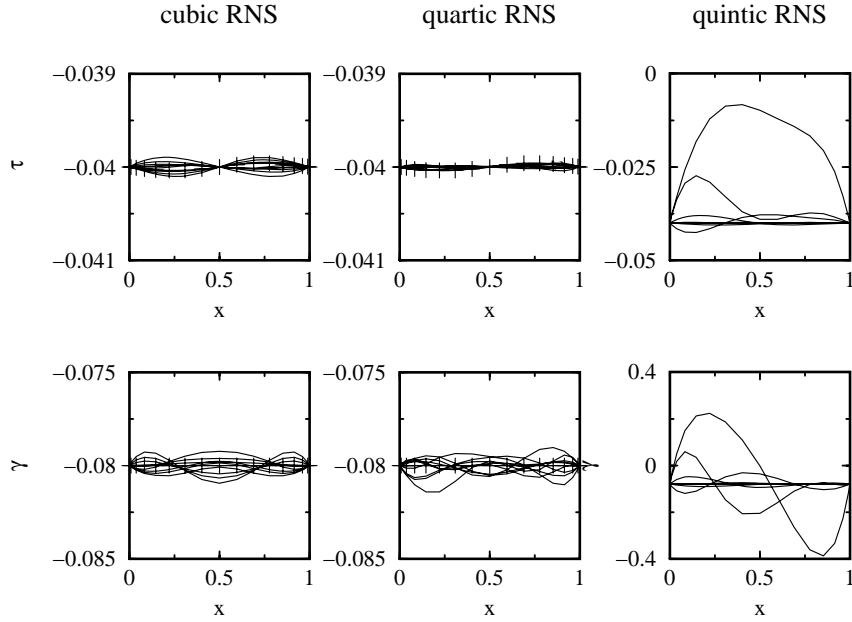


Figure 3: Evolution of the  $\tau$  and  $\gamma$  profiles in the cubic, quartic, and quintic RNS equations for the channel flow. The snapshots are taken with nondimensional time step  $\Delta\bar{t} = 0.1$ ; the final simulation time is  $\bar{t} = 10$  for the cubic and quartic RNS equations, and  $\bar{t} = 7$  for the quintic RNS equation. Crosses mark the exact solution.

The boundary conditions for (38) are  $F(0) = F' = 0$  and  $F'(\infty) = 1$ . Solving (38) numerically with these boundary conditions yields  $F''(0) = 1.23259$ . From the velocity expression (37), we find that

$$\begin{aligned} \tau_{\text{exact}}(x) &= B\rho\sqrt{\nu B}F''(0)x, & \gamma_{\text{exact}}(x) &= -B^2\rho x, & \sigma_v(x) &= 0.0, \\ \lambda_{\text{exact}}(x) &= \frac{B^4\rho}{\nu}[F''(0)]^2 x, & \eta_{\text{exact}}(x) &= -2\sqrt{\frac{B}{\nu}}\frac{B^4\rho}{\nu}F''(0)x. \end{aligned} \quad (39)$$

#### Validation

For the numerical solution of the RNS equations, we obtain initial and boundary conditions from (39). We solve the equations on the spatial domain  $x \in [0, 1m]$  with  $B = 1 \text{ s}^{-1}$  and  $\nu = 10^{-2} \text{ m}^2/\text{s}$ ; the corresponding Reynolds number is  $\text{Re} = 100$ , which is well within the validity of the laminar stagnation flow approximation.

Figure 6 again shows limited error growth. In this simulation, however, the 1% error bar is reached in 0.1 nondimensional time units, indicating faster error growth than in earlier examples. While the quartic RNS is an order of magnitude more accurate for  $\gamma$  than the cubic RNS, the two sets of equations perform equally well for  $\tau$ . The quintic model shows a much improved estimation for the evolution of  $\tau$ .

As for qualitative accuracy, we show the time evolution of the  $\tau$  and  $\gamma$  profiles in Fig. 7. In all cases, qualitative closeness to the approximate analytic solution is maintained for convective times up to  $\bar{t} = 1$ .

## Fluid oscillation over an infinite plate

### Analytical solution

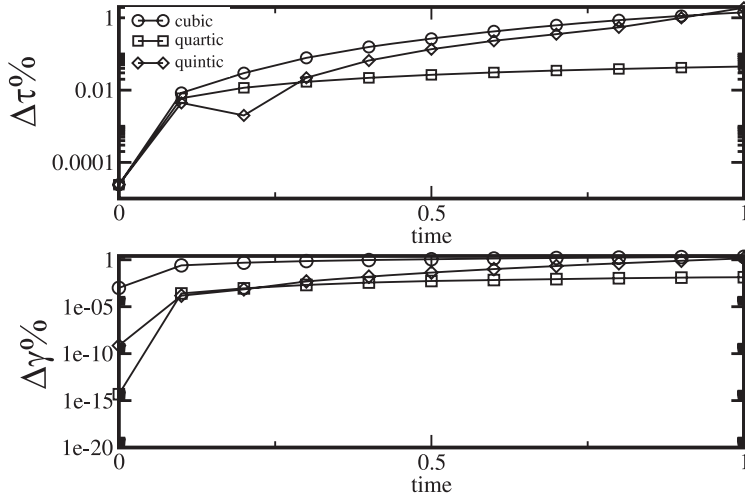


Figure 4: Percentage of error in  $\tau$  and  $\gamma$  as a function of time for the Blasius profile.

For an unsteady parallel laminar flow, the Navier-Stokes equations reduce to

$$u_t = -\frac{1}{\rho}p_x + \nu u_{yy}. \quad (40)$$

The pressure gradient can only be a function of time for this flow, and hence can be absorbed into the velocity by a change of variables leading to a homogeneous diffusion equation (White [13]).

For an oscillating wall with  $u(0, t) = U_0 \cos \omega t$  with zero velocity far from the wall, the velocity field is of the form  $u(y, t) = f(y)e^{i\omega t}$ . Substitution into the above-mentioned diffusion equation leads to  $f = e^{-\eta} \cos(\omega t - \eta)$ , where  $\eta = y\sqrt{\frac{\omega}{2\nu}}$ . The real part of  $u(y, t)$  is then given by

$$u(y, t) = U_0 e^{-\eta} \cos(\omega t - \eta). \quad (41)$$

With (41) at hand, we find that

$$\begin{aligned} \tau_{\text{exact}}(x) &= -\rho\nu B[\cos \omega t - \sin \omega t], \\ \gamma_{\text{exact}}(x) &= -2\rho\nu B^2 \sin \omega t, \\ \sigma_{\text{exact}}(x) &= 2\rho\nu B^3[\sin \omega t - \cos \omega t], \\ \lambda_{\text{exact}}(x) &= -4\rho\nu B^4 \cos \omega t, \\ \eta_{\text{exact}}(x) &= 4\rho\nu B^5[\cos \omega t - \sin \omega t], \end{aligned} \quad (42)$$

where  $B = \sqrt{\omega/(2\nu)}$ . Note that all the above quantities are independent of  $x$ .

#### Validation

Again, (42) provide initial and boundary conditions for our RNS simulations. We select  $U_0 = 1$  m/s,  $\nu = 10$  m<sup>2</sup>/s, and  $\omega = \pi$  1/s; we solve the cubic, quartic and quintic RNS equations for  $0 \leq x \leq 1$  m. The corresponding Reynolds number is  $\text{Re} = 0.1$ , which is consistent with the Stokes-flow approximation present in (40). Figure 8 shows that the  $L_2$  error in  $\tau$  and  $\gamma$  remains below 3% for up to 0.1 nondimensional time unit. In addition, the quartic model predicts  $\gamma$  two orders of magnitude more accurately than the cubic model.

In this example, we observe qualitative correctness for the RNS systems on long time scales. Shown in Fig. 9, the  $\tau$  and  $\gamma$  profiles stay qualitatively close to the exact solution for up to 4 nondimensional time units; the errors appear uniformly bounded for all times.

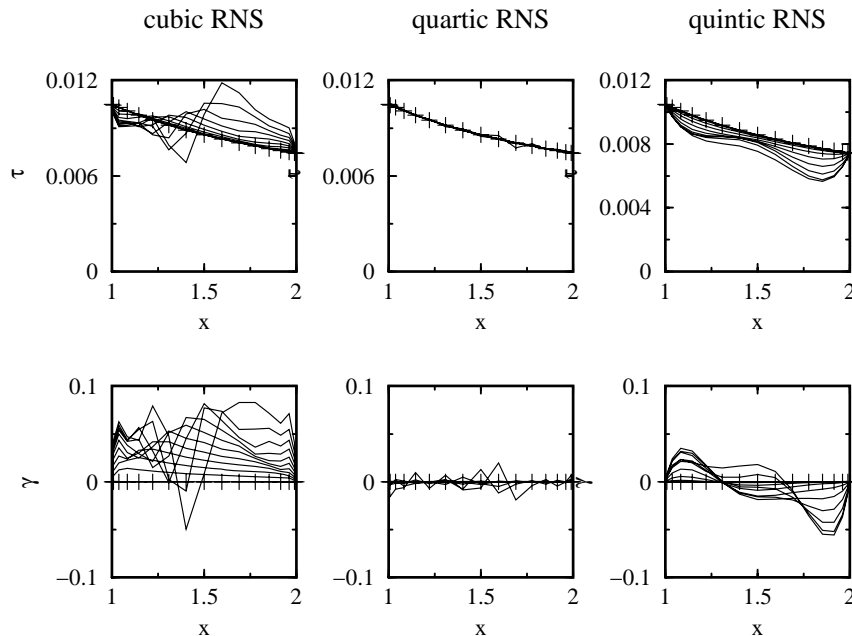


Figure 5: Evolution of the  $\tau$  and  $\gamma$  profiles in the cubic, quartic, and quintic RNS equations for the Blasius boundary layer flow. The snapshots are taken with nondimensional time step  $\Delta\bar{t} = 0.3$ ; the final simulation time is  $\bar{t} = 3$ . Crosses mark the exact solution.

## 5.1 Steady and unsteady lid-driven cavity flow

As our final example, we use direct numerical simulation of a lid-driven cavity to test the accuracy of the RNS equations. The simulations are performed with a staggered-grid multidomain spectral method (Kopriva [8] and Jacobs et al. [9]). The computational model consists of a square whose upper boundary is a lid moving at a constant speed.

The Reynolds number  $Re = 400$  of the flow is based on the velocity of the lid and the length of the square's side. The flow is started from a quiescent state that develops into a steady state. The steady-state solution is characterized by three vortices, as shown by the streamlines in Fig. 10(a). This steady-state solution agrees with previously published results by Ghia et al. [4], as seen in Fig. 10(b).

At the steady state, we evaluate the  $y$ -derivatives of the velocity to be used as initial conditions for the RNS equations. The boundary conditions for the RNS equations at  $x = 0$  m and  $x = L = 1$  m are zero because of the zero derivatives at the corners of the cavity.

Figure 11 and 12 show that up to time  $\bar{t} = 1$ , the skin friction  $\tau$  remains within 1% of its steady state value for both the cubic and the quartic RNS equations. Over the same time period,  $\gamma$  shows errors in the order of 10%. Qualitative correctness holds up to time  $\bar{t} = 2$  for  $\gamma$ , and up to  $\bar{t} = 3$  for  $\tau$ .

Figure 13 compares  $\tau$  for the initial *unsteady* cavity flow. The velocity gradients at  $\bar{t} = 5.0$  are used as initial conditions for the RNS equations. At later times, the computed  $\tau$  values from the RNS equations are compared with the simulation. We find that at time  $\bar{t} = 5.1$ , the RNS equations compare reasonably with the simulation. Although at  $\bar{t} = 5.2$ , the RNS equations show substantial deviation from the Navier-Stokes simulation, the  $\tau$  profile is still qualitatively correct. With initial conditions re-set at  $\bar{t} = 5.1$ , the RNS equations again remain accurate for times of order 0.1; qualitative accuracy again persists somewhat longer, but is lost by  $\bar{t} = 5.5$ .

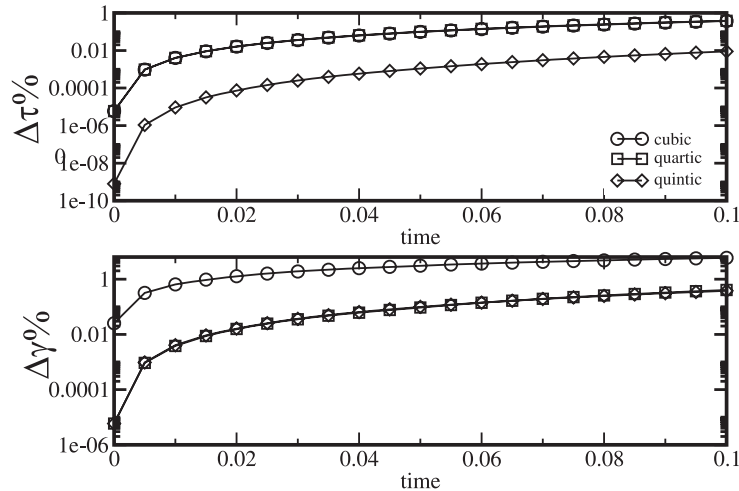


Figure 6: Percentage of error in  $\tau$  and  $\gamma$  as a function of time for the viscous stagnation point flow.

Finally, we compare the local  $u$ -velocity reconstructed from the truncated expansion (5) using the cubic and quartic RNS simulations. Figures 14 and 15 compare true and reconstructed  $u$  velocities at select  $x$  and  $y$  locations near the  $y = 0$  boundary during the initial unsteady phase of the cavity flow.

The conclusion from figures Figs. 14 and 15 is that the skin-friction and pressure-gradient evolution obtained from the RNS equations is suitable for short-term velocity field prediction near the wall away from corners. A general discussion on velocity reconstruction from instantaneous skin-friction and wall-pressure measurements is given by Bewley and Protas [12].

## 6 Conclusions

In this paper, we have derived a hierarchy of evolution equations for two key wall-based quantities, the skin friction and the wall-pressure gradient, in two-dimensional incompressible flows. The resulting RNS equations are well-posed for smooth enough initial data. Defined over the flow boundary, the RNS equations offer reduced spatial dimensionality over the full Navier-Stokes equations; as a result, typical computation times for the RNS equations are a fraction of those for the Navier-Stokes equations.

For instance, on a 2.2GHz Intel Xeon processor, our spectral Navier-Stokes simulation of the lid-driven cavity flow (programmed in Fortran90) required about 1 minute of CPU time to compute the velocity field over the convective time scale  $\Delta t = 0.2$ . By contrast, on a slower ULTRASPARC-III 750 MHz processor, our spectral RNS simulation of the same problem (programmed in MATLAB) required only about 1.4 seconds for the cubic RNS and 1.9 seconds for the quartic RNS equation. The RNS equations, however, rely on updated boundary conditions and hence cannot be solved without observing the flow at two discrete boundary points.

Our numerical simulations on a range of benchmark problems show quantitative accuracy for short-to-intermediate times: the RNS equations produced less than 1% error over times that range from 0.1 to 3 nondimensional time units in different problems. The error growth was noticeably faster

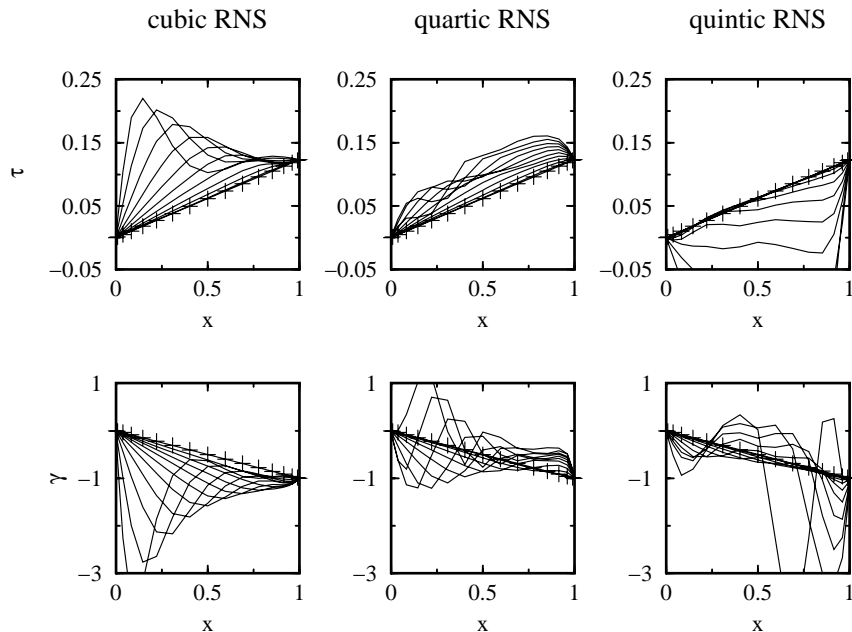


Figure 7: Evolution of the  $\tau$  and  $\gamma$  profiles in the cubic, quartic, and quintic RNS equations for the viscous stagnation point flow. The snapshots are taken with nondimensional time step  $\Delta \bar{t} = 0.1$ ; the final simulation time is  $\bar{t} = 1.5$ . Crosses mark the exact solution.

in the lid-driven cavity flow, where corner effects result in large wall-normal derivatives that are not captured by truncations of (5). In their envisioned application in flow control, however, the RNS equations should be more useful as qualitative reduced-order models rather than exact numerical tracking tools. In most of our examples, the RNS equations remained qualitatively accurate for times between 1 and 10 nondimensional time units. Over longer times, the equations require periodic re-initialization for sustained qualitative accuracy.

Our results are directly applicable in unsteady separation control when combined with the analytic approach of Alam, Liu and Haller [1]. In that approach, the solution of the skin-friction equation (7) was controlled via two-point boundary actuation to satisfy the kinematic separation conditions of Haller [6]. The velocity derivative  $\sigma$ , however, was obtained from observations rather than from a model. We expect an improvement in the controller derived in [1] once the present RNS equations are used to obtain predictions for  $\sigma$ . This is explored in ongoing work.

Reduced spatial dimensionality comes at a price: higher-order RNS equations include higher-order spatial derivatives, both in the equations and in the boundary conditions. Over a certain order, the computation of derivatives becomes too expensive and the advantage of reduced spatial dimensionality is lost. For this reason, we only expect the cubic and quartic RNS equations to be effective in flow-control applications, unless the equations are posed between boundary points with known velocity derivatives.

In the present work, we have tested the RNS equations numerically for Reynolds numbers up to  $10^3$ . In this range, assuming a two-dimensional flow geometry is reasonable for a number of applications. The behavior of the RNS hierarchy for higher Reynolds numbers is expected to be more delicate. We plan to study this question in future work.

Three-dimensional extensions of the present work are possible as our initial results indicate in section 3. In that case, the RNS equations are defined over two-dimensional boundary domains and hence require boundary conditions observed along one-dimensional curves. Such observations

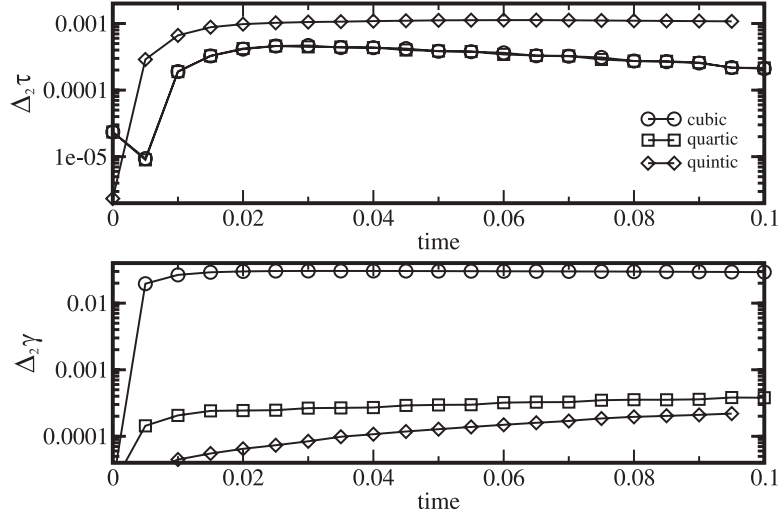


Figure 8:  $L_2$  error in  $\tau$  and  $\gamma$  as a function of time for flow oscillating over an infinite plate.

are possible via two-dimensional arrays of skin-friction and pressure sensors, thus applications to three-dimensional flow modelling and control appear feasible.

#### Acknowledgement

We thank Tom Bewley and Miroslav Krstic for useful discussions and insights. This work was supported by AFOSR Grant F49620-03-1-0200 and NSF Grant DMS-04-04845. In addition, the work of G.B.J. and J.S.H. was partially supported by NSF Career Award DMS0132967.

## 7 Appendix A: Well-posedness for the RNS equations

### 7.1 Well-posedness for the cubic RNS equations

#### 7.1.1 Function space

We consider the PDE system (14) with the boundary conditions (15). We will first show that (14) has a unique solution for the homogeneous boundary conditions

$$\tau(0, t) = \tau(L, t) = 0, \quad \gamma(0, t) = \gamma(L, t) = 0, \quad \sigma(0, t) = \sigma(L, t) = 0, \quad (43)$$

on the function space

$$X = B^3 \times B^2 \times B^1,$$

where

$$B^n = \{u \in H^n([0, L]) : u(0) = u(L) = 0\}. \quad (44)$$

On the space  $X$ , we define the norm

$$\begin{aligned} \|U\|^2 &= \|(\tau, \gamma, \sigma)\|^2 = \int_0^L \{|\tau|^2 + |\tau_x|^2 + |\tau_{xx}|^2 + |\tau_{xxx}|^2 + |\gamma|^2 + |\gamma_x|^2 + |\sigma|^2 + |\sigma_x|^2\} dx \\ &= \langle \tau, \tau \rangle + \langle \tau_x, \tau_x \rangle + \langle \tau_{xx}, \tau_{xx} \rangle + \langle \tau_{xxx}, \tau_{xxx} \rangle + \langle \gamma, \gamma \rangle + \langle \gamma_x, \gamma_x \rangle + \langle \sigma, \sigma \rangle + \langle \sigma_x, \sigma_x \rangle \\ &= \langle \langle \tau, \tau \rangle \rangle_3 + \langle \langle \gamma, \gamma \rangle \rangle_1 + \langle \langle \sigma, \sigma \rangle \rangle_1, \end{aligned} \quad (45)$$

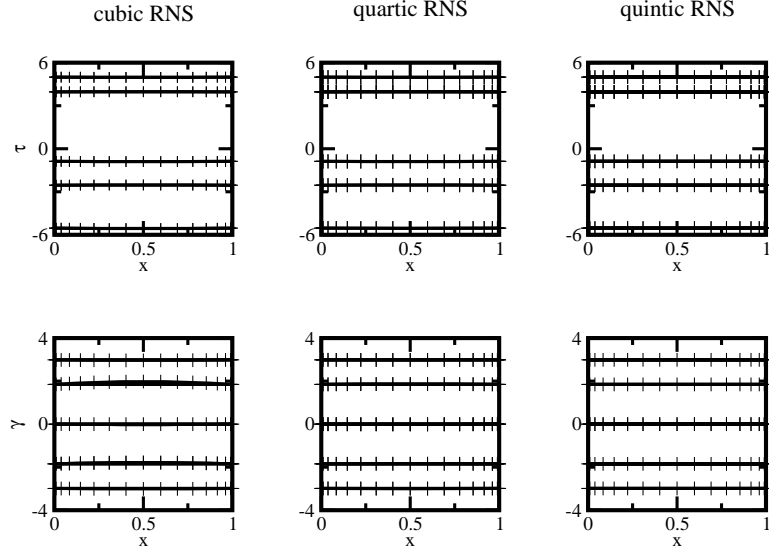


Figure 9: Evolution of the  $\tau$  and  $\gamma$  profiles in the cubic, quartic, and quintic RNS equations for the oscillating plate flow. The snapshots are taken with nondimensional time step  $\Delta \bar{t} = 0.4$ ; the final simulation time is  $\bar{t} = 4$ . Crosses mark the exact solution.

where  $\langle\langle v, v \rangle\rangle_n = \langle v, v \rangle + \langle v_x, v_x \rangle + \langle v_{xx}, v_{xx} \rangle + \dots + \langle \partial_x^n v, \partial_x^n v \rangle$ .

The homogeneous boundary conditions (43) and the equations (14) imply

$$\tau_{xx}(0) = \tau_{xx}(L) = 0, \quad \gamma_{xx}(0) = \gamma_{xx}(L) = 0. \quad (46)$$

Differentiating the first equation in (14) twice, we obtain

$$\tau_{xxt} = 2\nu\tau_{xxxx} + \nu\sigma_{xx},$$

which gives

$$\begin{aligned} 0 &= 2\nu\tau_{xxxx}(0) + \nu\sigma_{xx}(0), \\ 0 &= 2\nu\tau_{xxxx}(L) + \nu\sigma_{xx}(L), \end{aligned}$$

by (43). Combining these last two equations with the third equation in (14) leads to

$$\sigma_{xx}(0) = \sigma_{xx}(L) = 0, \quad \tau_{xxxx}(0) = \tau_{xxxx}(L) = 0. \quad (47)$$

### 7.1.2 Evolution equation formulation

Next we rewrite system (14) in the evolution equation form

$$u_t = Au + f(u), \quad (48)$$

where

$$A = \begin{pmatrix} 2\nu\partial_{xx} & 0 & \nu \\ 0 & 2\nu\partial_{xx} & 0 \\ -\nu\partial_{xxxx} & 0 & \nu\partial_{xx} \end{pmatrix}, \quad f(u) = \begin{pmatrix} 0 \\ -\frac{1}{\nu\rho}\tau\tau_x \\ -\frac{2}{\nu\rho}\tau\gamma_x \end{pmatrix}. \quad (49)$$

By a classic result of Pazy [10], the linear operator  $A$  is the infinitesimal generator of a  $C^0$  semigroup  $T(t)$  with  $\|T(t)\| \leq Me^{\omega t}$ , if  $A$  satisfies the following conditions:

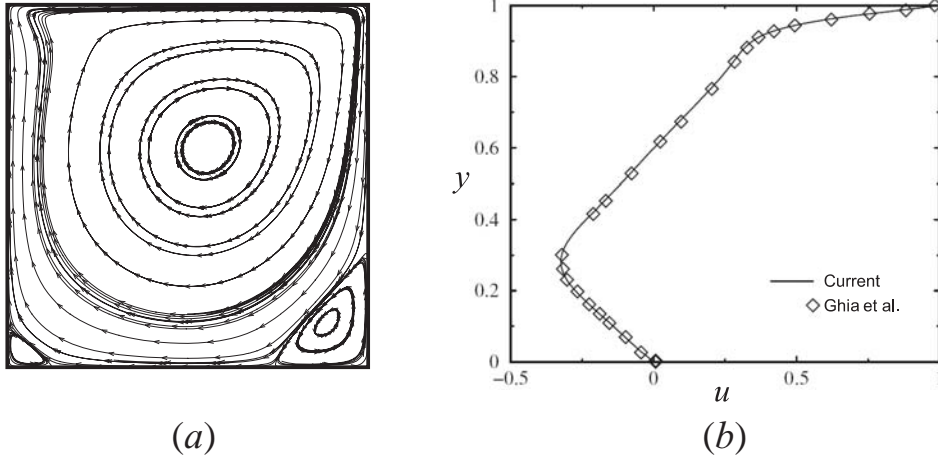


Figure 10: (a) Streamlines at the steady state of a lid-driven cavity flow at  $Re = 400$ . (b) Comparison of a  $u$ -velocity profile along the midplane for the steady state of a lid-driven cavity at  $Re = 400$ .

- (i)  $A$  is closed and the domain of  $A$ ,  $D(A)$ , is dense in  $X$ .
- (ii) The resolvent set  $\rho(A) = \left\{ \lambda \in \mathbb{C} : (\lambda I - A)^{-1} \text{ exists} \right\}$  of  $A$  contains an interval  $(\omega, \infty)$  such that for all  $\lambda > \omega$ , the resolvent operator

$$R_A(\lambda) = (\lambda I - A)^{-1} \quad (50)$$

satisfies

$$\|R_A^n(\lambda)\| \leq M(\lambda - \omega)^{-n}. \quad (51)$$

Since  $A$  is a linear combination of closed differential operators,  $A$  is closed. Moreover, the domain of  $A$  contains  $C^\infty \times C^\infty \times C^\infty$  which is dense in  $X$ . Hence, the conditions in (i) are satisfied.

To show that (ii) is also satisfied, we have to identify the spectrum of  $A$ . To this end, we expand  $\tau$ ,  $\gamma$ , and  $\sigma$  into Fourier series:

$$\tau = \sum_{n=1}^{\infty} a_n \sin k_n x, \quad \gamma = \sum_{n=1}^{\infty} b_n \sin k_n x, \quad \sigma = \sum_{n=1}^{\infty} c_n \sin k_n x.$$

(Here we have implicitly extended all three functions to the interval  $[-L, 0]$  in an odd manner.) Using (46) and (47), we obtain

$$\begin{aligned} \tau_{xx} &= -\sum_{n=1}^{\infty} k_n^2 a_n \sin k_n x, & \tau_{xxxx} &= \sum_{n=1}^{\infty} k_n^4 a_n \sin k_n x, \\ \gamma_{xx} &= -\sum_{n=1}^{\infty} k_n^2 b_n \sin k_n x, & \sigma_{xx} &= -\sum_{n=1}^{\infty} k_n^2 c_n \sin k_n x, \end{aligned} \quad (52)$$

after integration by parts. Here the equality signs are meant in the sense of  $L_2$  convergence; the wave number is  $k_n = 2n\pi/L$ .

By (49) and (52), the spectrum of  $A$  is the union of the spectra of the three-by-three matrices

$$A_{k_n} = \begin{pmatrix} -2\nu k_n^2 & 0 & \nu \\ 0 & -2\nu k_n^2 & 0 \\ -\nu k_n^4 & 0 & -\nu k_n^2 \end{pmatrix},$$

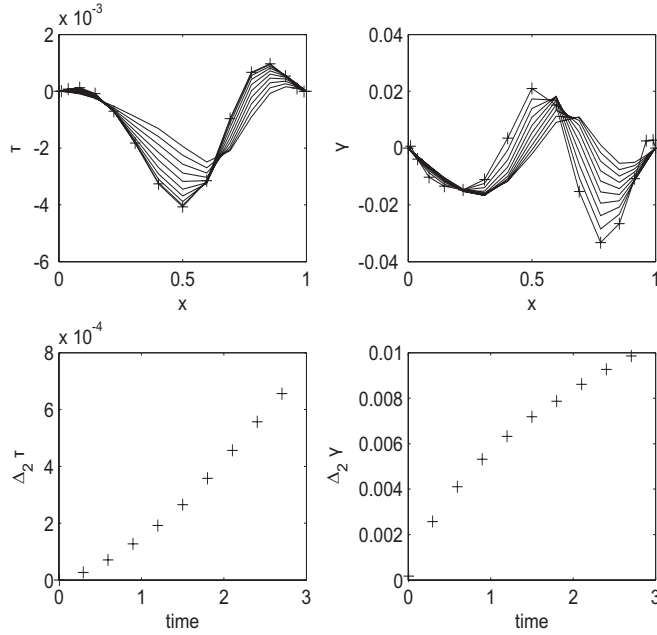


Figure 11: Errors in the cubic RNS simulation of the lid-driven cavity flow. The (absolute) errors  $\Delta\tau$  and  $\Delta\gamma$  are shown as functions of the location for different times; the  $L_2$ -errors  $\Delta_2\tau$  and  $\Delta_2\gamma$  are shown as functions of the nondimensionalized time.

which are found to be

$$\sigma(A_{k_n}) = \left\{ -2\nu k_n^2, \left( -\frac{3}{2} \pm i\frac{\sqrt{3}}{2} \right) \nu k_n^2 \right\}.$$

Therefore, the spectrum of  $A$  lies in the negative complex half-plane bounded away from zero.

Although the spectrum of  $A$  is confined to the negative complex half-plane,  $A$  is not self-adjoint, and hence we cannot directly conclude the boundedness of  $\exp(At)$  from its boundedness in eigenbasis. Establishing well-posedness for (48), therefore, requires more than just the boundedness of the spectrum of the linear part. For instance, the linear system

$$\begin{aligned} u_t &= Au, \\ u(x, 0) &= u_0(x), \end{aligned}$$

with  $A$  defined in (49) is *not* well-posed on the space  $\tilde{X} = L^2 \times L^2 \times L^2$ , because the norm of

$$\exp(A_{k_n} t) = e^{-\frac{3}{2}k_n^2 t} \begin{pmatrix} \frac{2}{\sqrt{3}} \cos\left(\frac{\sqrt{3}}{2}k_n^2 t + \frac{\pi}{6}\right) & 0 & \frac{2}{\sqrt{3}k_n^2} i k_n^{-2} \sin\left(\frac{\sqrt{3}}{2}k_n^2 t\right) \\ 0 & e^{-\frac{1}{2}k_n^2 t} & 0 \\ \frac{2}{\sqrt{3}} i k_n^2 \sin\left(\frac{\sqrt{3}}{2}k_n^2 t\right) & 0 & \frac{2}{\sqrt{3}} \cos\left(\frac{\sqrt{3}}{2}k_n^2 t - \frac{\pi}{6}\right) \end{pmatrix}$$

does not admit a  $k$ -independent upper bound of the form  $Ke^{\alpha t}$  (cf. Gustaffson et al. [5]).

We proceed by defining

$$F = (\lambda I - A)U,$$

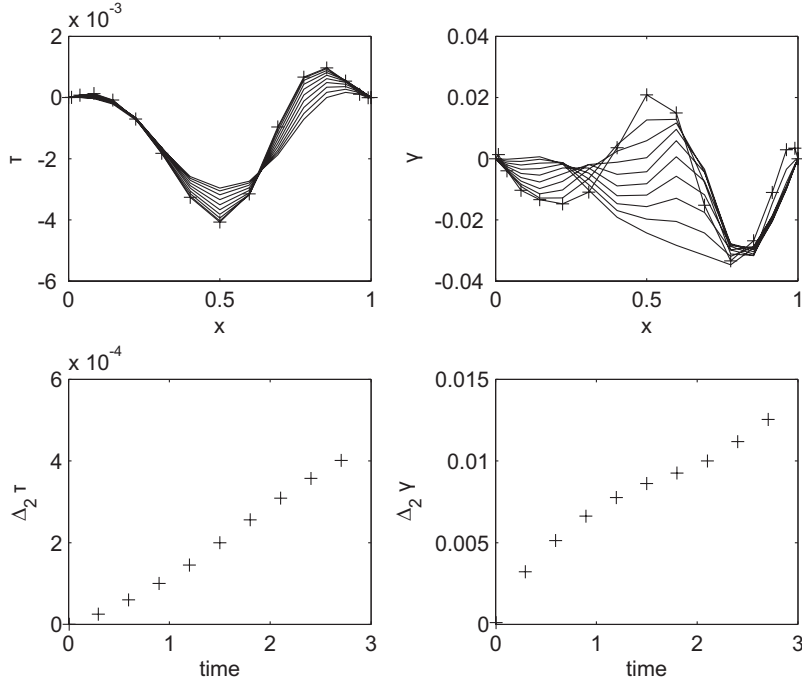


Figure 12: Same as Fig. 11, but for the quartic RNS simulation of the lid-driven cavity flow.

or, in component form,

$$\begin{aligned}
 f_1 &= \lambda\tau - 2\nu\tau_{xx} - \nu\sigma, \\
 f_2 &= \lambda\gamma - 2\nu\gamma_{xx}, \\
 f_3 &= \lambda\sigma - \nu\sigma_{xx} + \nu\tau_{xxx}.
 \end{aligned}$$

The norm of  $F$  can then be written as

$$\begin{aligned}
 \|F\|^2 &= \langle\langle f_1, f_1 \rangle\rangle_3 + \langle\langle f_2, f_2 \rangle\rangle_2 + \langle\langle f_3, f_3 \rangle\rangle_1 \\
 &= \langle\langle \lambda\tau - 2\nu\tau_{xx} - \nu\sigma, \lambda\tau - 2\nu\tau_{xx} - \nu\sigma \rangle\rangle_3 + \langle\langle \lambda\gamma - 2\nu\gamma_{xx}, \lambda\gamma - 2\nu\gamma_{xx} \rangle\rangle_2 \\
 &\quad + \langle\langle \lambda\sigma - \nu\sigma_{xx} + \nu\tau_{xxx}, \lambda\sigma - \nu\sigma_{xx} + \nu\tau_{xxx} \rangle\rangle_1.
 \end{aligned} \tag{53}$$

We find that

$$\begin{aligned}
 &\langle\langle \lambda\tau - 2\nu\tau_{xx} - \nu\sigma, \lambda\tau - 2\nu\tau_{xx} - \nu\sigma \rangle\rangle_3 \\
 &= \lambda^2 \langle\langle \tau, \tau \rangle\rangle_3 + 2\lambda\nu \langle\langle \tau, -2\tau_{xx} - \sigma \rangle\rangle_3 + \langle\langle 2\tau_{xx} - \sigma, 2\tau_{xx} - \sigma \rangle\rangle_3 \\
 &= \lambda^2 \langle\langle \tau, \tau \rangle\rangle_3 - 2\lambda\nu \langle\langle \tau, \sigma \rangle\rangle_3 + 4\lambda\nu \langle\langle \tau_x, \tau_x \rangle\rangle_3 + \langle\langle 2\tau_{xx} - \sigma, 2\tau_{xx} - \sigma \rangle\rangle_3 \\
 &\geq \lambda^2 \langle\langle \tau, \tau \rangle\rangle_3 - 2\lambda\nu \langle\langle \tau, \sigma \rangle\rangle_3,
 \end{aligned} \tag{54}$$

and

$$\begin{aligned}
 \langle\langle \lambda\gamma - 2\nu\gamma_{xx}, \lambda\gamma - 2\nu\gamma_{xx} \rangle\rangle_2 &= \lambda^2 \langle\langle \gamma, \gamma \rangle\rangle_2 - 4\nu\lambda \langle\langle \gamma, \gamma_{xx} \rangle\rangle_2 + 4\nu^2 \langle\langle \gamma_{xx}, \gamma_{xx} \rangle\rangle_2 \\
 &= \lambda^2 \langle\langle \gamma, \gamma \rangle\rangle_2 + 4\nu\lambda \langle\langle \gamma_x, \gamma_x \rangle\rangle_2 + 4\nu^2 \langle\langle \gamma_{xx}, \gamma_{xx} \rangle\rangle_2 \\
 &\geq \lambda^2 \langle\langle \gamma, \gamma \rangle\rangle_2;
 \end{aligned} \tag{55}$$

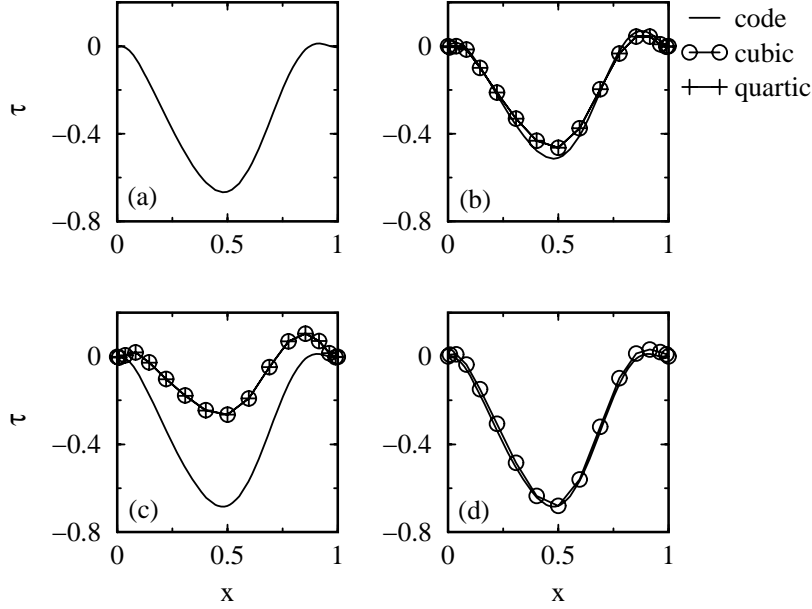


Figure 13: Comparison of skin-friction values predicted by a Navier-Stokes simulation (“code”), and by the cubic and quartic RNS simulation for the initial unsteady phase of the lid-driven cavity flow at  $\text{Re} = 400$ . (a) Initial condition at  $\bar{t} = 5.0$  (b) Simulation at  $\bar{t} = 5.1$  (c) simulation at  $\bar{t} = 5.2$  (d) Same as (c) but with initial conditions re-initialized at  $\bar{t} = 5.1$ .

furthermore,

$$\begin{aligned}
& \langle \langle \lambda \sigma - \nu \sigma_{xx} + \nu \tau_{xxxx}, \lambda \sigma - \nu \sigma_{xx} + \nu \tau_{xxxx} \rangle \rangle_1 \\
&= \lambda^2 \langle \langle \sigma, \sigma \rangle \rangle_1 - 2\lambda\nu \langle \langle \sigma, \sigma_{xx} \rangle \rangle_1 + 2\lambda\nu \langle \langle \sigma, \tau_{xxxx} \rangle \rangle_1 + \langle \langle \nu \sigma_{xx} + \nu \tau_{xxxx}, \nu \sigma_{xx} + \nu \tau_{xxxx} \rangle \rangle_1 \\
&\geq \lambda^2 \langle \langle \sigma, \sigma \rangle \rangle_1 + 2\lambda\nu \langle \langle \sigma, \tau_{xxxx} \rangle \rangle_1 = \lambda^2 \langle \langle \sigma, \sigma \rangle \rangle_1 + 2\lambda\nu \langle \langle \sigma_{xx}, \tau_{xx} \rangle \rangle_1 \\
&\geq \lambda^2 \langle \langle \sigma, \sigma \rangle \rangle_1 + 2\lambda\nu [\langle \langle \sigma, \tau \rangle \rangle_3 - \langle \langle \sigma, \tau \rangle \rangle_1].
\end{aligned} \tag{56}$$

Using the estimates (54)-(56) in (53), we obtain

$$\begin{aligned}
\|F\|^2 &\geq \lambda^2 \langle \langle \tau, \tau \rangle \rangle_3 - 2\lambda\nu \langle \langle \tau, \sigma \rangle \rangle_3 + \lambda^2 \langle \langle \gamma, \gamma \rangle \rangle_2 + \lambda^2 \langle \langle \sigma, \sigma \rangle \rangle_1 + 2\lambda\nu [\langle \langle \sigma, \tau \rangle \rangle_3 - \langle \langle \sigma, \tau \rangle \rangle_1] \\
&= \lambda^2 \langle \langle \tau, \tau \rangle \rangle_3 + \lambda^2 \langle \langle \gamma, \gamma \rangle \rangle_2 + \lambda^2 \langle \langle \sigma, \sigma \rangle \rangle_1 - 2\lambda\nu \langle \langle \sigma, \tau \rangle \rangle_1 \\
&\geq \lambda^2 \langle \langle \tau, \tau \rangle \rangle_3 + \lambda^2 \langle \langle \gamma, \gamma \rangle \rangle_2 + \lambda^2 \langle \langle \sigma, \sigma \rangle \rangle_1 - \lambda\nu [\langle \langle \sigma, \sigma \rangle \rangle_1 + \langle \langle \tau, \tau \rangle \rangle_1] \\
&\geq (\lambda^2 - \lambda\nu) \|U\|^2 \geq (\lambda - \nu)^2 \|U\|^2
\end{aligned}$$

for all  $\lambda > \nu$ .

Thus, for all  $\lambda > \nu$ , we obtain

$$\frac{\|U\|}{\|F\|} \leq \frac{1}{\lambda - \nu}.$$

Consequently, the resolvent  $R_A(\lambda)$  defined in (50) satisfies

$$\|R_A(\lambda)\| \leq \frac{1}{\lambda - \nu},$$

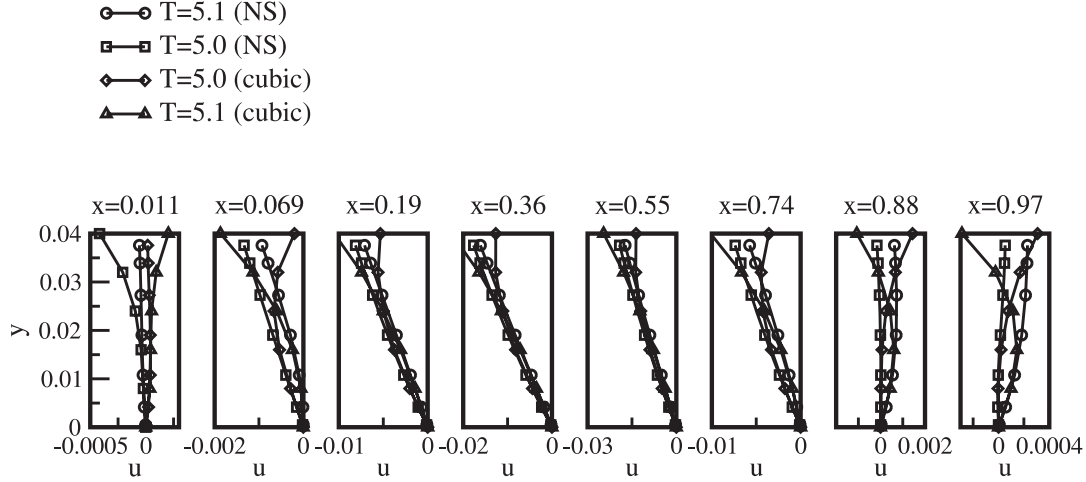


Figure 14: The  $u$ -component of the lid-driven cavity velocity field at  $\bar{t} = 5.0$  and  $\bar{t} = 5.1$  at different locations near the  $y = 0$  boundary. “NS” refers to Navier-Stokes simulations; “cubic” refers to cubic RNS simulations.

or, equivalently,

$$\|R_A^n(\lambda)\| \leq \|R_A(\lambda)\|^n \leq \frac{1}{(\lambda - \nu)^n}.$$

We, therefore, conclude that property (51) is satisfied for  $\omega \equiv \nu > 0$ , and hence  $A$  is an infinitesimal generator of a  $C^0$  semigroup  $T(t)$  with

$$\|T(t)\| \leq e^{\nu t}.$$

### 7.1.3 Existence for the full cubic RNS equations

For system (48), Pazy [10] shows that if  $A$  is the infinitesimal generator of a  $C^0$  semigroup on  $X$ , and  $f : X \rightarrow X$  is continuously differentiable, then (48) has a unique (classical) solution  $u$  over the time interval  $[t_0, t_{\max})$ . Moreover, if  $t_{\max} < \infty$ , then  $\lim_{t \rightarrow t_{\max}} \|u(t)\| = \infty$ .

We have already shown that  $A$  is an infinitesimal generator of a  $C^0$  semigroup. We now prove that  $f(u)$  is continuously differentiable in  $u$ . We first observe that  $f$  is defined and uniformly continuous on a dense subset of the complete space  $X = B^1([0, L]) \times B^2([0, L]) \times B^2([0, L])$ . As a result,  $f$  can be extended continuously to the whole of  $X$ .

For  $u = (\tau, \gamma, \sigma)$  and  $h = (h_1, h_2, h_3) \in X$ , we can write

$$f(u+h) - f(u) = -\frac{1}{\nu\rho} \begin{pmatrix} 0 \\ h_1\tau_x + h_{1x}\tau + h_1h_{1x} \\ 2(\tau h_{2x} + h_{1x}\gamma_x + h_1h_{2x}) \end{pmatrix},$$

which gives

$$D_u f(u) = -\frac{1}{\nu\rho} \begin{pmatrix} 0 & 0 & 0 \\ \tau_x + \tau \frac{d}{dx} & 0 & 0 \\ 2\gamma_x & 2\tau \frac{d}{dx} & 0 \end{pmatrix},$$

a map continuous in  $X$  with respect to the norm  $\|\cdot\|$  defined in (45). Therefore, the cubic RNS equations with homogeneous boundary conditions are well posed: they have unique classical solutions that depend continuously on the initial conditions.

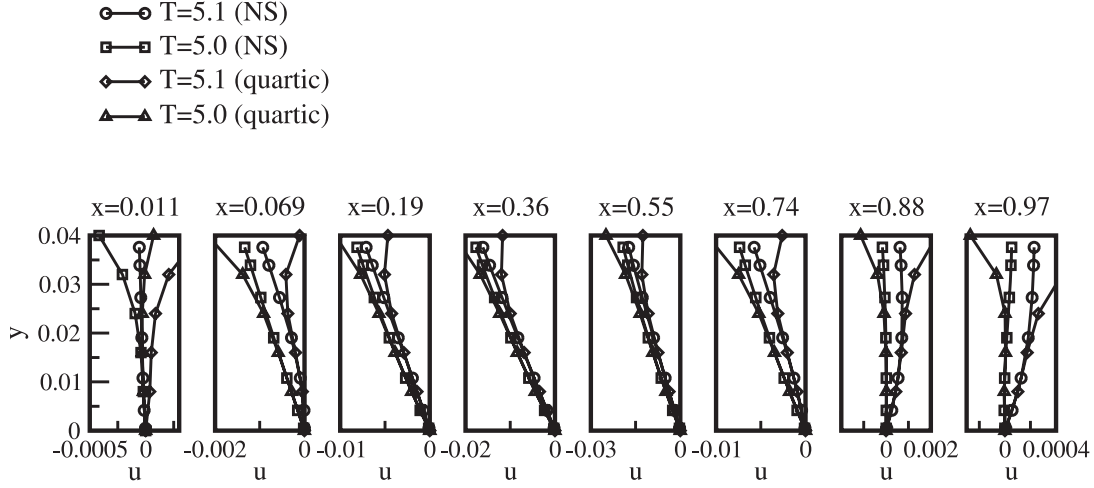


Figure 15: Same as Fig. 14, but for the quartic RNS simulation.

#### 7.1.4 Inhomogeneous boundary conditions

We reconsider the system (14) with the boundary and initial conditions (15). Under the change of variables

$$\begin{aligned}\tau &= \tau' + \frac{1}{L}[(L-x)T_0(t) + xT_L(t)] = \tau' + F(x, t), \\ \gamma &= \gamma' + \frac{1}{L}[(L-x)p_x(0, t) + xp_x(L, t)] = \gamma' + P(x, t), \\ \sigma &= \sigma' + \frac{1}{L}[(L-x)S_0(t) + xS_L(t)] = \sigma' + H(x, t),\end{aligned}$$

system (14) becomes

$$\begin{aligned}\tau'_t &= 2\nu\tau'_{xx} + \nu\sigma' + \nu H - F_t, \\ \gamma'_t &= 2\nu\gamma'_{xx} - \frac{1}{\nu\rho}\tau'\tau'_x - \frac{1}{\nu\rho}\tau'F_x - \frac{1}{\nu\rho}F\tau'_x - \frac{1}{\nu\rho}FF_x - P_t, \\ \sigma'_t &= \nu\sigma'_{xx} - \nu\tau'_{xxxx} - \frac{2}{\nu\rho}\tau'\gamma'_x - \frac{2}{\nu\rho}\tau'P_x - \frac{2}{\nu\rho}F\gamma'_x - \frac{2}{\nu\rho}FP_x - S_t.\end{aligned}\tag{57}$$

which has a different linear part than (14) does. However, we can view (57) as

$$u_t = Au + g(u),$$

where  $A$  is given in (49) and  $g$  has quadratic, linear and constant terms in  $u$ . It is straightforward to check that  $g$  is continuously differentiable on  $X$ , thus all our previous arguments remain valid, and the existence of a unique solution with continuous dependence on initial data is proved.

## 7.2 Existence and uniqueness for higher-order RNS equations

### 7.2.1 The linear part

To derive the  $n$ th equation of the RNS system of order  $N$  with  $N \geq n \geq 3$ , we take the  $(n-3)$ rd  $y$ -derivative of equation (10), then subtract from that the second  $x$ -derivative of the  $(n-2)$ nd-order RNS equation. Carrying out this procedure for only the linear parts of the equations, we obtain the linear part of the  $n$ th order RNS equation, which we explore below.

With the notation

$$u^n = \rho \nu \frac{\partial^n u}{\partial y^n},$$

the linear part of (10) becomes

$$\partial_t(u^3 + \partial_x^2 u^1) = 2\nu \partial_x^2 u^3 + \nu u^5 + \partial_x^4 u^1.$$

Taking  $(n-3)$ rd derivative of this last equation with respect to  $y$ , we obtain

$$\partial_t(u^n + \partial_x^2 u^{n-2}) = 2\nu \partial_x^2 u^n + \nu u^{n+2} + \partial_x^4 u^{n-2}. \quad (58)$$

This last equation is also valid for  $n = 1, 2$ , except that the terms containing  $u^{n-2}$  are absent. Taking the second  $x$ -derivative of (58) and letting  $n \rightarrow n-2$ , we find that

$$\partial_t(\partial_x^2 u^{n-2} + \partial_x^4 u^{n-4}) = 2\nu \partial_x^4 u^{n-2} + \nu \partial_x^2 u^n + \partial_x^6 u^{n-4}. \quad (59)$$

Subtracting (58) from (59), we obtain

$$\partial_t(u^n - \partial_x^4 u^{n-4}) = \nu \partial_x^2 u^n + \nu u^{n+2} - \partial_x^4 u^{n-2} - \partial_x^6 u^{n-4}. \quad (60)$$

Next, we add to (60) the equation

$$\partial_t(\partial_x^4 u^{n-4} + \partial_x^6 u^{n-6}) = 2\nu \partial_x^6 u^{n-4} + \nu \partial_x^4 u^{n-2} + \partial_x^8 u^{n-6},$$

which we obtain from (58) by taking the 4th  $x$ -derivative and letting  $n \rightarrow n-4$ . The resulting equation is

$$\partial_t(u^n + \partial_x^6 u^{n-6}) = \nu \partial_x^2 u^n + \nu u^{n+2} + \partial_x^6 u^{n-4} + \partial_x^8 u^{n-6}, \quad (61)$$

in which the order of the  $y$ -derivative on the left-hand side has decreased by 2 compared to (60).

We repeat the above order-reduction procedure until only  $\partial_t u^n$  is left on the left-hand side of the equation. This happens when the superscript of  $u$  in the second term of the left-hand side reaches  $-1$  or  $-2$ ; this indicates that that corresponding term is absent.

In the case of  $n = 4k + i$  with  $i = 1, 2$ , the resulting linear equation is

$$u_t^n = \nu \partial_x^2 u^n + \nu u^{n+2} + \nu \partial_x^{n-i+2} u^i;$$

in the case of  $n = 4k + 2 + i$  with  $i = 1, 2$ , the resulting linear equation is

$$u_t^n = \nu u_{xx}^n + \nu u^{n+2} - \nu \partial_x^{n-i+2} u^i.$$

When  $n+2 > N$ , the term containing the superscript  $n+2$  is absent, because we truncate the Taylor-expansion of  $u$  at order  $N$ .

In summary, the *linear* part of the  $N$ th order RNS system, say in the case of  $N = 4K + 1$ , is of the form

$$\begin{aligned}
u_t^1 &= 2\nu\partial_x^2 u^1 + \nu u^3, \\
u_t^2 &= 2\nu\partial_x^2 u^2 + \nu u^4, \\
u_t^3 &= \nu\partial_x^2 u^3 + \nu u^5 + \nu\partial_x^4 u^1, \\
u_t^4 &= \nu\partial_x^2 u^4 + \nu u^6 + \nu\partial_x^4 u^2, \\
&\vdots \\
u_t^{4k+i} &= \nu\partial_x^2 u^{4k+i} + \nu u^{4k+i+2} + \nu\partial_x^{4k+2} u^i, \\
u_t^{4k+i+2} &= \nu\partial_x^2 u^{4k+i+2} + \nu u^{4k+i+4} + \nu\partial_x^{4k+4} u^i, \\
&\vdots \\
u_t^{4K} &= \nu\partial_x^2 u^{4K} + \nu\partial_x^{4K} u^2, \\
u_t^{4K+1} &= \nu\partial_x^2 u^{4K+1} + \nu\partial_x^{4K+2} u^1,
\end{aligned} \tag{62}$$

where  $i = 1, 2$ , and all terms are evaluated at  $y = 0$ . The structure of the RNS system for other values of  $N$  is similar.

We consider the  $N$ th order RNS system (62) on the function space

$$X = B^N \times B^{N-1} \times \dots \times B^2 \times B^1,$$

where  $B^n$  is defined in (44). On  $X$ , we define the norm

$$\|U\|^2 = \{\langle u^1, u^1 \rangle\}_N + \frac{1}{\sqrt{2}} \langle u^2, u^2 \rangle_{N-1} + \frac{1}{2} \{\langle u^3, u^3 \rangle\}_{N-2} + \langle u^4, u^4 \rangle_{N-3} + \dots + \frac{1}{2^{(N-1)/2}} \langle u^{2k+i}, u^{2k+i} \rangle_1,$$

where  $i = 1$  or  $2$ , and

$$\langle u, v \rangle_n = \langle u, v \rangle + \langle u_x, v_x \rangle + \langle u_{xx}, v_{xx} \rangle + \dots + \langle \partial_x^n u, \partial_x^n v \rangle.$$

We observe that the homogeneous boundary conditions imply

$$\begin{aligned}
\partial_x^2 u^N &= 0, & \partial_x^2 u^{N-1} &= 0, \\
\partial_x^{2j+2} u^{N-2} &= 0, & \partial_x^{2j+2} u^{N-3} &= 0, & j &= 0, 1, \\
\partial_x^{2j+2} u^{N-4} &= 0, & \partial_x^{2j+2} u^{N-5} &= 0, & j &= 0, 1, 2, \\
&\vdots \\
\partial_x^{2j+2} u^1 &= 0, & j &= 0, 1, 2, \dots, m = (N-1)/2.
\end{aligned}$$

We again let

$$F = (\lambda I - A)U,$$

where  $A$  is the linear operator appearing on the right-hand side of the RNS system (62). We estimate

the norm of  $F$  as

$$\begin{aligned}
\|F\|^2 &= \langle\langle f_1, f_1 \rangle\rangle_N + \frac{1}{\sqrt{2}} \langle\langle f_2, f_2 \rangle\rangle_{N-1} + \frac{1}{2} \langle\langle f_3, f_3 \rangle\rangle_{N-2} + \dots + \frac{1}{2^{(N-1)/2}} \langle\langle f_N, f_N \rangle\rangle \\
&= \langle\langle \lambda u^1 - 2\nu \partial_x^2 u^1 - \nu u^3, \lambda u^1 - 2\nu \partial_x^2 u^1 - \nu u^3 \rangle\rangle_N \\
&\quad + \frac{1}{\sqrt{2}} \langle\langle \lambda u^2 - 2\nu \partial_x^2 u^2 - \nu u^4, \lambda u^2 - 2\nu \partial_x^2 u^2 - \nu u^4 \rangle\rangle_{N-1} \\
&\quad + \frac{1}{2} \langle\langle \lambda u^3 - \nu \partial_x^2 u^3 + \nu \partial_x^4 u^1 - \nu u^5, \lambda u^3 - \nu \partial_x^2 u^3 + \nu \partial_x^4 u^1 - \nu u^5 \rangle\rangle_{N-2} \\
&\quad + \frac{1}{2\sqrt{2}} \langle\langle \lambda u^4 - \nu \partial_x^2 u^4 + \nu \partial_x^4 u^2 - \nu u^6, \lambda u^4 - \nu \partial_x^2 u^4 + \nu \partial_x^4 u^2 - \nu u^6 \rangle\rangle_{N-3} \\
&\quad + \frac{1}{4} \langle\langle \lambda u^5 - \nu \partial_x^2 u^5 + \nu \partial_x^6 u^1 - \nu u^7, \lambda u^5 - \nu \partial_x^2 u^5 + \nu \partial_x^6 u^1 - \nu u^7 \rangle\rangle_{N-4} \\
&\quad + \dots \\
&\quad + \frac{1}{2^{(N-1)/2}} \langle\langle \lambda u^N - \nu \partial_x^2 u^N + \nu \partial_x^4 u^{N-2} \pm \nu \partial_x^{N-i+2} u^i, \lambda u^N - \nu \partial_x^2 u^N + \nu \partial_x^4 u^{N-2} \pm \nu \partial_x^{N-i+2} u^i \rangle\rangle_1 \\
&\geq \lambda^2 \langle\langle u^1, u^1 \rangle\rangle_N + 2\lambda\nu \langle\langle \partial_x u^1, \partial_x u^1 \rangle\rangle_N - 2\lambda\nu \langle\langle u^1, u^3 \rangle\rangle_N + \dots \\
&\quad + \frac{1}{2} \lambda^2 \langle\langle u^3, u^3 \rangle\rangle_{N-2} + \lambda\nu \langle\langle \partial_x u^3, \partial_x u^3 \rangle\rangle_{N-2} - \lambda\nu \langle\langle u^3, u^5 \rangle\rangle_{N-2} + \lambda\nu \langle\langle \partial_x^2 u^3, \partial_x^2 u^1 \rangle\rangle_{N-2} + \dots \\
&\quad + \frac{1}{4} \lambda^2 \langle\langle u^5, u^5 \rangle\rangle_{N-4} + \frac{1}{2} \lambda\nu \langle\langle \partial_x u^5, \partial_x u^5 \rangle\rangle_{N-4} - \frac{1}{2} \lambda\nu \langle\langle u^5, u^7 \rangle\rangle_{N-4} + \frac{1}{2} \lambda\nu \langle\langle \partial_x u^5, \partial_x^5 u^1 \rangle\rangle_{N-4} + \dots \\
&\quad \vdots \\
&\quad + \frac{1}{2^{(N-1)/2}} \{ \lambda^2 \langle\langle u^N, u^N \rangle\rangle_1 + 2\lambda\nu \langle\langle \partial_x u^N, \partial_x u^N \rangle\rangle_1 \\
&\quad \quad - 2\lambda\nu \langle\langle \partial_x u^N, \partial_x^3 u^{N-2} \rangle\rangle_1 + 2\lambda\nu \langle\langle \partial_x u^N, \partial_x^{N-i+1} u^i \rangle\rangle_1 \}
\end{aligned} \tag{63}$$

Based on the estimates

$$\begin{aligned}
|-\lambda\nu \langle\langle u^1, u^3 \rangle\rangle + \lambda\nu_N \langle\langle \partial_x^2 u^3, \partial_x^2 u^1 \rangle\rangle_{N-2}| &= |-\lambda\nu \langle\langle u^1, u^3 \rangle\rangle_1| \\
&\leq \frac{1}{2} \lambda\nu [\langle\langle u^1, u^1 \rangle\rangle_1 + \langle\langle u^3, u^3 \rangle\rangle_1], \\
|\langle\langle u^1, u^3 \rangle\rangle_N| &= |\langle\langle \partial_x^2 u^1, \partial_x^2 u^3 \rangle\rangle_{N-2}| + |\langle\langle u^1, u^3 \rangle\rangle_1| \\
&= |\langle\langle \partial_x^3 u^1, \partial_x u^3 \rangle\rangle_{N-2}| + |\langle\langle u^1, u^3 \rangle\rangle_1| \\
&\leq \frac{1}{2} [\langle\langle \partial_x^3 u^1, \partial_x^3 u^1 \rangle\rangle_{N-2} + \langle\langle \partial_x u^3, \partial_x u^3 \rangle\rangle_{N-2}] + |\langle\langle u^1, u^3 \rangle\rangle_1| \\
&\leq \frac{1}{2} [\langle\langle \partial_x u^1, \partial_x u^1 \rangle\rangle_N + \langle\langle \partial_x u^3, \partial_x u^3 \rangle\rangle_{N-2} + \langle\langle u^3, u^3 \rangle\rangle_1], \\
\langle\langle \partial_x u^5, \partial_x^5 u^1 \rangle\rangle_{N-4} &\leq \frac{1}{2} [\langle\langle \partial_x u^5, \partial_x u^5 \rangle\rangle_{N-4} + \langle\langle \partial_x^5 u^1, \partial_x^5 u^1 \rangle\rangle_{N-4}] \\
&\leq \frac{1}{2} [\langle\langle \partial_x u^5, \partial_x u^5 \rangle\rangle_{N-4} + \langle\langle \partial_x u^1, \partial_x u^1 \rangle\rangle_N],
\end{aligned}$$

we deduce the general relations

$$\begin{aligned}
\langle\langle u^n, u^{n+2} \rangle\rangle_{N+1-n} &\leq \frac{1}{2} [\langle\langle u^{n+2}, u^{n+2} \rangle\rangle_{N-1-n} + \langle\langle u^n, u^n \rangle\rangle_{N+1-n}], \\
\langle\langle \partial_x u^n, \partial_x^n u^1 \rangle\rangle_{N+1-n} &\leq \frac{1}{2} [\langle\langle \partial_x u^n, \partial_x u^n \rangle\rangle_{N+1-n} + \langle\langle \partial_x u^1, \partial_x u^1 \rangle\rangle_N].
\end{aligned}$$

Combining these last two inequalities with (63), we find that for  $\lambda > 0$ ,

$$\|F\|^2 \geq (\lambda^2 - \lambda\nu) \|U\|^2 \geq (\lambda - \nu)^2 \|U\|^2,$$

which again implies

$$\|R_A^n(\lambda)\| \leq \|R_A(\lambda)\|^n \leq \frac{1}{(\lambda - \nu)^n}.$$

Therefore, property (51) is again satisfied for the resolvent of  $A$ , and hence for  $\omega \equiv \nu > 0$ , the linear system (62) admits a  $C^0$  semiflow  $T(t)$  with

$$\|T(t)\| \leq e^{\nu t}.$$

This proves the existence, uniqueness and  $C^0$  regularity of solutions of the  $N$ th-order linearized RNS system.

### 7.2.2 The full nonlinear system

We now extend the above regularity result to the full  $N$ th-order RNS system

$$u_t = Au + f(u), \quad (64)$$

where  $Au$  represents the right-hand side of (62), and  $f(u)$  denotes the quadratic terms. By the result of Pazy [10], system (64) is well-posed if  $f: X \rightarrow X$  is continuously differentiable.

Let  $\{\mathbf{e}_i\}_{i=1}^N$  be the standard basis of  $\mathbb{R}^N$ . We observe that by the definition of the space  $X$ , the map

$$f_{l,m_1,n_1,m_2,n_2}: X \rightarrow X, \quad (65)$$

$$u \mapsto \mathbf{e}_l (\partial_x^{m_1} u^{n_1}) (\partial_x^{m_2} u^{n_2}), \quad (66)$$

is continuously differentiable if

$$m_1 \leq l - n_1, \quad m_2 \leq l - n_2. \quad (67)$$

All terms in the  $N$ th-order RNS system are of the general form (65); a systematic review of these terms reveals that they all satisfy (67). (We omit a detailed listing of the nonlinear terms for brevity.)

We conclude that the function  $f(u)$  in (64) is continuously differentiable, and hence the  $N$ th-order RNS system with homogeneous boundary conditions admits unique solutions that are continuous with respect to the initial data. The case of inhomogeneous boundary conditions follows as in the case of the cubic RNS system (cf. Appendix 7.1).

## 8 Appendix B: Derivation of the cubic RNS equations in 3D

Subtracting the  $x$ -derivative of the third equation in (22) from the  $z$ -derivative of the first equation, we obtain

$$\begin{aligned} & \partial_t(u_z - w_x) + u_{xz}u + u_xu_z + u_{yz}v + u_yv_z + u_{zz}w \\ & + u_zw_z - w_{zx}u - w_xu_z - w_{yz}v - w_yv_z - w_{zz}w - w_zw_z \\ & = \nu(u_{xxz} + u_{yyz} + u_{zzz} - w_{xxx} - w_{yyx} - w_{zzx}). \end{aligned} \quad (68)$$

Evaluating (68) at  $z = 0$  and using the no-slip boundary conditions, we obtain

$$[u_{zt}]_{z=0} = [\nu u_{zzz} + \nu u_{zxx} + \nu u_{zyy} - \nu w_{zzx}]_{z=0}.$$

By incompressibility, this last equation yields

$$[u_{zt}]_{z=0} = [2\nu u_{zxx} + \nu u_{zyy} + \nu v_{zxy} + \nu u_{zzz}]_{z=0}. \quad (69)$$

The same argument applied to the  $v$ -component of the Navier-Stokes equations gives

$$[v_{zt}]_{z=0} = [2\nu v_{zyy} + \nu v_{zxx} + \nu u_{zxy} + \nu v_{zzz}]_{z=0}. \quad (70)$$

We continue by taking the  $z$ -derivative of equation (68) to obtain

$$\begin{aligned} & \partial_t(u_{zz} - w_{zx}) + u_{zzz}u + 2u_{zx}u_z + u_xu_{zz} + u_{zzy}v + 2u_{zy}v_z + vu_yv_{zz} + u_{zzz}w + 2u_{zz}w_z \\ & + u_zw_{zz} - w_{zzx}u - 2w_{zx}u_z - w_xu_{zz} - w_{yzz}v - 2w_{yz}v_z - w_yv_{zz} - w_{zzz}w - 3w_{zz}w_z \\ = & \nu(u_{zzzx} + u_{zzyy} + u_{zzzz} - w_{zxxx} - w_{zyyx} - w_{zzzx}). \end{aligned} \quad (71)$$

Evaluation at  $z = 0$  then gives

$$[u_{zzt}]_{z=0} = [-2u_zu_{zx} - 2u_{zy}v_z - u_zw_{zz} + \nu(2u_{zzzx} + u_{zzyy} + u_{zzzz} + v_{zzxy})]_{z=0}.$$

We use incompressibility to rewrite this last equation as

$$[u_{zzt}]_{z=0} = [\nu(2u_{zzzx} + u_{zzyy} + u_{zzzz} + v_{zzxy}) - u_zu_{zx} - 2u_{zy}v_z - u_zv_{zy}]_{z=0}. \quad (72)$$

Similarly, we obtain

$$[v_{zzt}]_{z=0} = [\nu(2v_{zzyy} + v_{zzzx} + v_{zzzz} + u_{zzxy}) - v_zv_{zy} - 2v_{zx}u_z - v_zu_{zx}]_{z=0}. \quad (73)$$

Differentiation of (71) with respect to  $z$  gives

$$\begin{aligned} & \partial_t(u_{zzz} - w_{zzx}) + u_{zzzx}u + 3u_{zzx}u_z + 3u_{zx}u_{zz} + u_xu_{zzz} + u_{zzzy}v + 3u_{zzy}v_z + 3u_{zy}v_{zz} \\ & + u_yv_{zzz} + u_{zzz}w + 3u_{zzz}w_z + 3u_{zz}w_{zz} + u_zw_{zzz} - w_{zzx}u - 3w_{zzx}u_z - 3w_{zx}u_{zz} - w_xu_{zzz} \\ & - w_{yzzz}v - 3w_{yz}v_z - 3w_{yz}v_{zz} - w_yv_{zzz} - w_{zzzz}w - 4w_{zzz}w_z - 3w_{zz}w_{zz} \\ = & \nu(u_{zzzx} + u_{zzzy} + u_{zzzz} - w_{zxxx} - w_{zyyx} - w_{zzzx}), \end{aligned}$$

which, at  $z = 0$ , becomes

$$\begin{aligned} [u_{zzzt} - w_{zzxt}]_{z=0} = & [-3u_{zzx}u_z - 3u_{zx}u_{zz} - 3u_{zzy}v_z - 3u_{zy}v_{zz} - 3u_{zz}w_{zz} - u_zw_{zzz} \\ & + 3w_{zzx}u_z + 3w_{yz}v_z + w_{zzz}w + 4w_{zzz}w_z + 3w_{zz}w_{zz} \\ & + \nu(u_{zzzx} + u_{zzzy} + u_{zzzz} - w_{zxxx} - w_{zyyx} - w_{zzzx})]_{z=0}. \end{aligned}$$

Imposing incompressibility on this last equation, we find that

$$\begin{aligned} [u_{zzzt}]_{z=0} = & -u_{zxt} - v_{xyt} - 3u_{zzx}u_z - 3u_{zx}u_{zz} - 3u_{zzy}v_z - 3u_{zy}v_{zz} + 3u_{zz}u_{zx} \\ & + 3u_{zz}v_{zy} + u_zu_{zzx} + u_zv_{zzy} - 3u_{zxx}u_z - 3v_{zxy}u_z + 3u_{zxy}v_z + 3v_{zyy}v_z + 3u_{zx}u_{zx} \\ & + 6u_{zx}v_{zy} + 3v_{zy}v_{zy} + \nu(u_{zzzx} + u_{zzzy} + u_{zzzz} - u_{zxxx} - v_{zyxx} - u_{zxyx}) \\ & - \nu(v_{zyyx} + u_{zzzx} + v_{zzzy})]_{z=0} \end{aligned} \quad (74)$$

Using (70), we can rewrite (74) as

$$\begin{aligned} [u_{zzzt}]_{z=0} = & [-\nu(2u_{zxxx} + u_{zyyx} + v_{zyyx} + u_{zzzx}) - \nu(2v_{zyyy} + v_{zxxx} + u_{zxyy} + v_{zzzy}) \\ & - 3u_{zzx}u_z - 3u_{zx}u_{zz} - 3u_{zzy}v_z \\ & - 3u_{zy}v_{zz} + 3u_{zz}u_{zx} + 3u_{zz}v_{zy} + u_zu_{zzx} + u_zv_{zzy} - 3u_{zxx}u_z - 3v_{zxy}u_z + 3u_{zxy}v_z \\ & + 3v_{zyy}v_z + 3u_{zx}u_{zx} + 6u_{zx}v_{zy} + 3v_{zy}v_{zy} \\ & + \nu(u_{zzzx} + u_{zzzy} + u_{zzzz} - u_{zxxx} - v_{zyxx} - u_{zxyx} - v_{zyyy} - u_{zzzx} - v_{zzzy})]_{z=0}. \end{aligned}$$

After cancellations due to incompressibility, the above equation becomes

$$\begin{aligned} [u_{zzzt}]_{z=0} = & [-\nu(3u_{zxxx} + 3u_{zyyx} + u_{zzzx} + 3v_{zxxx}) \\ & + 3v_{zyyy} + 2v_{zzzy} - u_{zzzy} - u_{zzzz}) \\ & - 2u_{zzx}u_z - 3u_{zzy}v_z - 3u_{zy}v_{zz} + 3u_{zz}v_{zy} \\ & + u_zv_{zzy} - 3u_{zxx}u_z - 3v_{zxy}u_z + 3u_{zxy}v_z \\ & + 3v_{zyy}v_z + 3u_{zx}u_{zx} + 6u_{zx}v_{zy} + 3v_{zy}v_{zy}]_{z=0}. \end{aligned} \quad (75)$$

A similar argument yields

$$\begin{aligned}
[v_{zzzt}]_{z=0} &= [-\nu(3v_{zyyyy} + 3v_{zyyx} + v_{zzzy} + 3u_{xyyy} \\
&\quad + 3u_{xxx} + 2u_{zzxy} - v_{zzzx} - v_{zzzz}) \\
&\quad - 2v_{zzy}v_z - 3v_{zzx}u_z - 3v_{zx}u_{zz} + 3v_{zz}u_{zx} \\
&\quad + v_zu_{zzx} - 3v_{zyy}v_z - 3u_{xy}v_z + 3v_{xy}u_z \\
&\quad + 3u_{zx}u_z + 3v_{zy}v_{zy} + 6v_{zy}u_{zx} + 3u_{zx}u_{zx}]_{z=0}.
\end{aligned} \tag{76}$$

Then equations (69), (70), (72), (73), (75), and (76) can be summarized as the cubic three-dimensional RNS system (24).

## References

- [1] Alam, M. R., Liu, W., and Haller, G., Closed-loop separation control: An analytic approach. *Phys. Fluids. A* (2005) submitted
- [2] Canuto, C., Hussaini, M. Y., Quarteroni, A., and Zang, T., *Spectral Methods in Fluid Dynamics*, Springer, New York (1987).
- [3] Danielson, T. J., and Ottino, J. M., Structural stability in two-dimensional model flows: Lagrangian and Eulerian turbulence. *Phys. Fluids. A* **2** (1990) 2024-2035.
- [4] Ghia, U., Ghia, K. N., and Shin, C.T., High-Re solutions for incompressible flow using the Navier-Stokes equations and a multigrid method. *J. Comp. Phys.* **48** (1982) 387-411.
- [5] Gustaffson, B., Kreiss, H.-O., and Olinger, J., *Time-Dependent Problems and Difference Methods*. Wiley, New York (1995).
- [6] Haller, G., Exact theory of unsteady separation for two-dimensional flows, *J. Fluid. Mech.* **512** (2004) 257-311.
- [7] Kelley, C. T., *Solving Nonlinear Equations with Newton's Method*. SIAM, Philadelphia (2003).
- [8] Kopriva, D. A., A staggered-grid multidomain spectral domain for the compressible Navier-Stokes equations, *J. Comp. Phys.*, **143** (1998) 125-158.
- [9] Jacobs, G.B., Kopriva, D. A., and Mashayek, F., Validation study of a multidomain spectral element code for simulation of turbulent flows, *AIAA J.*, (2004), in press.
- [10] Pazy, A., *Semigroups of Linear Operators and Applications to Partial Differential Equations*. Springer, New York (1983).
- [11] Perry, A. E. & Chong, M. S. A series-expansion study of the Navier-Stokes Equations with applications to three-dimensional unsteady flow, *J. Fluid. Mech.* **173** (1986) 207-223.
- [12] Bewley, T. R. & Protas, B., Skin friction and pressure: The footprints of turbulence. *Physica D* **196** (2004) 28-44.
- [13] White, F. M., *Viscous Fluid Flow*. McGraw-Hill, Singapore (1991).